FISEVIER

Contents lists available at ScienceDirect

Palaeogeography, Palaeoclimatology, Palaeoecology

journal homepage: www.elsevier.com/locate/palaeo





Palaeoenvironmental changes and anthropogenic impact recorded in floodplain sediments: A case study from the lower Morava River Basin (Czech Republic)

Jaroslav Kadlec ^{a,1}, Ivo Světlík ^b, Michal Rybníček ^{c,d}, Tomáš Kolář ^{c,d}, Filip Stehlík ^e, Eduard Petrovský ^{a,*}, Hana Grison ^a

- ^a Institute of Geophysics CAS, Boční II/1401, 14100 Prague 4, Czech Republic
- ^b Nuclear Physics Institute CAS, CRL Radiocarbon Laboratory, Na Truhlárce 39/64, 18086 Prague 6, Czech Republic
- c Department of Wood Science and Wood Technology, Faculty of Forestry and Wood Technology, Mendel University in Brno, 61300 Brno, Czech Republic
- d Global Change Research Institute of the Czech Academy of Sciences, 60300 Brno, Czech Republic
- ^e Modenská 663/1, 10900 Prague 10, Czech Republic

ARTICLE INFO

Editor: Paul Hesse

Keywords: Strážnické pomoraví Flood frequency Soil erosion Human activities Magnetic minerals Radiocarbon dating Dendrochronology

ABSTRACT

The Morava River catchment in the Czech Republic serves as sedimentary archive reflecting various natural and man-made processes, and was studied by several authors from the point of view of flood frequency, anthropogenic contamination, or alluvial history. However, more consistent and detailed information on the effect of human activities, namely in terms of land use and river regulation, is missing. The aim of this study is to reconstruct the palaeoenvironmental and anthropogenic processes affecting the floodplain sediments in this area, focusing on the last few hundreds of years. Alluvial sediments from river banks and drilled cores were collected in the Strážnické pomoraví area from sites both inside and outside dams constructed to avoid flooding. Magnetic parameters, reflecting the composition and grain-size distribution of iron oxides, which serve as fingerprints of lithogenic vs. pedogenic vs. anthropogenic origin, are complemented by the radiocarbon and dendrochronological dating. In addition, deposition age was estimated using the ¹³⁷Cs activity and persistent organic pollutant content. Our results reveal continuous increase of ferrimagnetic minerals (magnetite) input to the floodplain, suggesting increased soil erosion in the catchment. Significantly different pattern was observed inside and outside the flood dykes. The erosion accelerated since the 1950s due to incorrect land use and introduction of modern agriculture techniques. Finally, the industrial pollution significantly contributes to the magnetic enhancement of the topmost 50 cm of the floodplain sequences. Although the results represent local case study, they have more general validity in the sense that records of paleoenvironmental changes and human activities in floodplain sediments may not be well preserved in all the strata, and also their spatial distribution of individual markers may show significant variability.

1. Introduction

Mineral magnetic studies are widely used as a tool for understanding the environmental processes as well as archaeological research interpretation and/or anthropogenically-induced pollution assessment (Dekkers, 1997). History of application of the mineral magnetic methods to sedimentary archives dates back to 1970s (Liu et al., 2012 and references herein). The methods were used in various settings (e.g.,

Thompson and Oldfield, 1986; Verosub and Roberts, 1997; Evans and Heller, 2004). In a continental realm, for instance, diagnostic changes of iron-bearing minerals in Pleistocene loess-palaeosol sequences reflect glacial/interglacial climatic variations, associated with interglacial soil formation controlled by summer monsoon rainfall oscillations (e.g., Liu and Ding, 1998; Maher, 2007, 2011). Correlation between magnetic susceptibility in the loess-palaeosol sequences and deep-sea oxygen isotope records is connected to the global palaeoclimate signals (Ding

E-mail addresses: svetlik@ujf.cas.cz (I. Světlík), michalryb@post.cz (M. Rybníček), koldatom@gmail.com (T. Kolář), edp@ig.cas.cz (E. Petrovský), grison@ig.cas.cz (H. Grison).

^{*} Corresponding author.

Passed away suddenly before the completion of the manuscript.

et al., 2002; Evans and Heller, 2004). Mineral magnetic variations recorded in lacustrine deposits often reflect relations between processes affecting both the provenance area and depositional site (e.g., Oldfield et al., 1983; Platzman and Lund, 2019).

The floodplain sedimentary archives can reflect natural and humaninduced processes influencing the river catchment. Such processes include soil evolution as well as unsuitable land use, which often trigger soil degradation, erosion, and re-deposition from the river catchment to the floodplain environment. All could play a significant role in mineral magnetic record stored in these floodplain sequences (e.g., Chaparro et al., 2011; Chaparro et al., 2013; Chaparro et al., 2015; Nováková et al., 2013; Chudaničová and Hutchinson, 2016; Chudaničová et al., 2016; Sedláček et al., 2019; Franke et al., 2020). Mineral magnetic techniques have been also applied to assessment of pollution using magnetic particles as tracers, often associated with increased heavy metal contamination due to fossil fuel combustion or traffic (e.g., Maher et al., 2008; Zhang et al., 2018; Wang et al., 2019), and are incorporated in the sedimentary archives (e.g., Magiera et al., 2011; Oldfield et al., 2015). The artificial spherical magnetite micro-particles are spread, together with other industrial emissions, over large areas and settled on the soil surface. During erosional events the pollutants are transported together with eroded soil by sheet flow to the streams and subsequently deposited in the floodplain environment (e.g., Knab et al., 2006; Sandeep et al., 2011; Fáměra et al., 2013).

Floodplain sediment aggradation and degradation are controlled by (i) stream discharge changes influenced by climatic factors such as precipitation and vegetation density in the stream catchment, (ii) tectonic movement controlling the river gradient, and/or (iii) human interventions including, e.g., forest clearance, intense land use, or canalizing the stream channel. Changes in these controlling mechanisms are responsible for evolution of river patterns related to characteristic fluvial activity (e.g., Charleton, 2008). The temperate central European floodplains are since the Late Glacial, when climate amelioration supported the vegetation development and the water discharge stabilization, characterized by meandering river systems (e.g., Kalicki, 2006). Meandering rivers are characterised by lateral shift of the channel cutting older floodplain deposits, and subsequently incorporating the eroded material into younger sedimentary beds, causing temporal and spatial reconstruction of the floodplain evolution more complicated (e. g., Kalicki and Krapiec, 1995). Recently, several multidisciplinary studies, involving sedimentological, geochemical, and geophysical approaches, were undertaken with the aim to reconstruct the evolution of the Morava River floodplain (e.g. Kadlec et al., 2009; Grygar et al., 2011, 2012, 2016; Bábek et al., 2011, 2018), as well as the history of soil erosion in controlling the sediment input to the floodplain (Nehyba et al., 2010a; Nehyba et al., 2010b). Floods history of the Morava River in relation to natural and man-made factors was studied by Brázdil et al. (2011a). For example, Brázdil et al. (2011a, 2011b) reported that flood frequency in this area was highest in the 1961-1970 decade. The frequency of floods and extent of floodplain inundations decreased after human interventions in 1930s. As regards the sedimentation rate, Grygar et al. (2011) concluded that this increased from 0.2-0.3 cm/year in 700 CE to 0.3-0.4 cm/year in 2000 CE. These values are much smaller than for other west and central European rivers, although the area has been intensively used for agriculture and its land cover has changed in a similar manner.

The Morava River floodplain archive should also record a significant period related to the first large settlement centers built in the floodplain during the 9th century. The contemporary inhabitants possibly affected the natural floodplain environmental balance by a large forest clearance around the settlements. These activities could change natural groundwater oscillation regime leading to frequent floods (Poláček, 2007).

The present study aims at the palaeoenvironmental reconstruction of the floodplain processes, controlled by both natural and anthropogenic events in the Morava River floodplain deposits, by combination of mineral magnetic methods and dating techniques. We intend to provide new information in addition to the results already published by, e.g., Brázdil et al. (2011a, 2011b), Grygar et al. (2010, 2011 and 2012) or Máčka and Kadlec (2016), in particular records related to the latest period and effects of change in land use and man-made regulation of the Morava River. In this sense, we build upon and extend significantly the results published by Kadlec et al. (2009).

2. Geographic and geological settings

The study area, Strážnické Pomoraví, is located in southern Moravia along the central course of the Morava River (Fig. 1). The river catchment area upstream of the Strážnické Pomoraví has 9146 km². Altitude of the study area is from 166 to 169 m a.s.l. (www.straznicko.cz, in Czech). The mean annual river discharge, measured at a gauge station Strážnice at Veselí nad Moravou (17.2976635°E, 48.933115°N), reaches 59.6 m³s⁻¹ (Máčka and Kadlec, 2016). The mean depositional rate between about 1000 to about 1900 CE is, depending on the sedimentary facies, from 0.2 to 0.6 mmy⁻¹ (Grygar et al., 2010). Average gradient of the river course is 0.13%. The length of the meandering channel of the Morava R. through the Strážnické Pomoraví area is approximately 12 km. The river has a 50-70 m wide channel incised into the floodplain sequences. The river channel was partly canalized across two meanders in 1939-42 (Smetana, 2011). As a consequence, the channel sinuosity has decreased from 1.60 to 1.31 and the river level incised down to 6 m below the floodplain surface. In 1937–38, the floodplain surface was artificially modified by flood dyke construction following the meander belt. Since then, the floodplain deposition has been mostly concentrated between the flood dykes (Máčka and Kadlec, 2016). More details on the channel network in Strážnické Pomoraví can be found in, e.g., Brázdil et al. (2011b).

The Holocene floodplain deposits up to 5 m thick are underlain with 5–8 m thick layer of fluvial sandy gravels, deposited during the last glacial stage. Bottom of the Morava R. valley is built up from the marine and continental Neogene sedimentary fill of the Vienna Basin (Havlíček and Smolíková, 1994; Havlíček et al., 2007). The catchment of the Morava River belongs to the principal fluvial systems of the Czech Republic, covering most of its eastern part, and geologically spanning the Paleozoic basement of the Bohemian Massif as well as part of the Western Carpathian orogen. While the area under consideration falls entirely within the Neogene fill of the Vienna Basin, the upper reaches of the Morava catchment drain a broad range of Paleozoic metamorphic and sedimentary units, as well as the Neogene Upper Morava Basin (Bábek et al., 2018).

Climate in the area is temperate, with the mean annual temperature of about 10 °C and mean annual precipitation between 585 and 600 mm (Brázdil et al., 2011b, www.straznicko.cz). Present land use (2002–2006) in the whole Morava River catchment is dominated by arable land (41.5%), forest (37.3%), permanent grassland (11.5%), and others (Brázdil et al., 2011a). Efforts to regulate the Morava River are dated back to 1653, when a decision to make the river navigable was made. The most significant effort was the construction of the Bata's Shipping Channel in 1934–1938 to transport lignite from the coal field downstream of the Strážnice area to factories in Otrokovice and Zlín upstream. Other projects were aiming at protection from floods (Brázdil et al., 2011a).

3. Material and methods

3.1. Studied sediment sections and sampling strategy

The floodplain deposits are exposed in the natural erosional river banks and are easily accessible. Modern point bar bodies, formed in new segments of the Morava R. channel canalized in the late 1930s, expose recently deposited sediments. The other sedimentary sections were obtained by drilling the floodplain fill in different distances from the river channel.

The sections exposed in the river banks were cleaned by removing

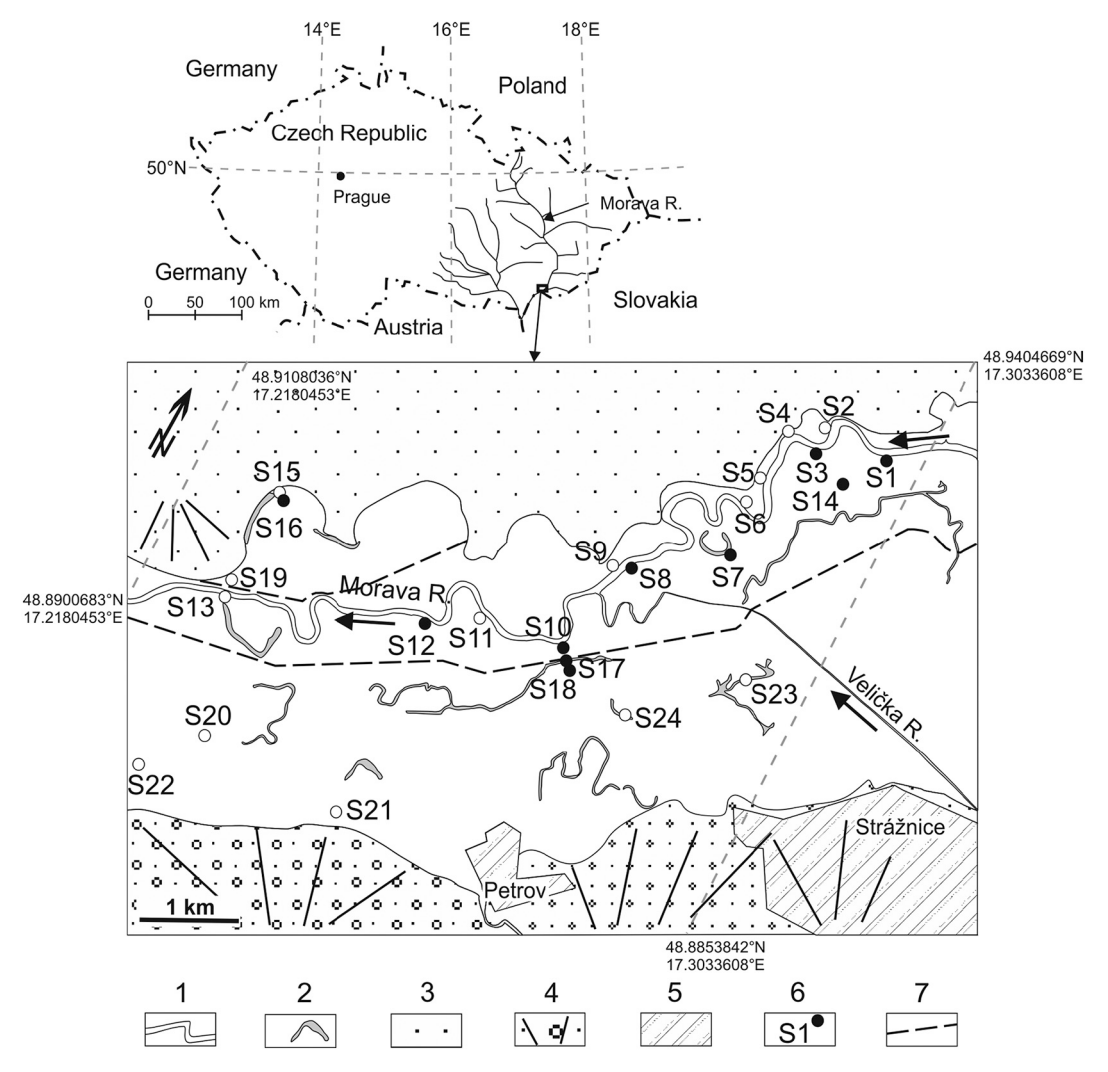


Fig. 1. Top: Location of the Morava River catchment with the Strážnické Pomoraví study area (rectangle). Arrows indicate the downstream direction. Bottom: Scheme of the study area. 1 - modern river bed, 2 - abandoned meander, 3 - lacustrine sand and sandy gravel covered by aeolian sandy dunes, 4 - Late and Mid-Pleistocene alluvial fans, 5- town, 6 - studied section (full dot – examined using magnetic and non-magnetic techniques, open dot – examined using non-magnetic techniques), 7 - flood dykes. Modified after Kadlec et al. (2009), © SAGE 2009.

about 0.5 m of material and subsequently were sampled between the floodplain surface and the low-stand water level. During the first sampling campaign (in summer 2006), the samples were collected from 3 pilot sections located at distances ~ 5 km downstream from one another along the Morava R. At each section, triplicate samples were collected at each stratigraphic level using plastic boxes (6.7 cm³ in volume) with a vertical spacing of less than 0.5 cm between sampling horizons. Later (October 2008 and 2009), the other sections, including the drilled cores, were sampled along vertical profile with spacing between 0.5 cm and 5 cm. All studied sediment sections (see Fig. 1) were carefully described and assessed from the river-dynamic point of view.

3.2. Laboratory techniques

3.2.1. Mineral magnetic analyses

Low-field volume-specific magnetic susceptibility (κ) was measured using both the MS2 Magnetic Susceptibility Meter (Bartington Instruments, sensitivity 2×10^{-6} SI) and the KLF4 Magnetic Susceptibility Meter (AGICO Ltd., sensitivity 1×10^{-6} SI). Bartington MS2 meter is a single-coil instrument, which is sensitive to temperature drift. Therefore, empty coil (air) was measured before and after specimen, and average of these two values was subtracted from the specimen measurement. In this way, each specimen was measured three times and

average value was calculated. The obtained values were transformed to mass-specific magnetic susceptibility (χ) using the sample weight after drying in air and assuming the standard measurement volume of $10~{\rm cm}^3$. This parameter reflects, in specimens of the same composition of iron oxides, mostly concentration of ferrimagnetic minerals (magnetite, maghemite). Frequency-dependent magnetic susceptibility (χ fd%) was determined on the basis of the MS2 Magnetic Susceptibility Meter measurements at frequencies of 0.465 and 4.65 kHz, expressed as percent change relative to the value measured at the lower frequency. This parameter is sensitive to relative amount of ultrafine, nano-sized superparamagnetic ferrimagnets, produced mostly by pedogenic processes (Dearing et al., 1996). Temperature dependence of susceptibility was measured using the AGICO Meter from room temperature up to 700 °C. Shape of the curves reflects composition of the specimens in terms of magnetic phases.

The susceptibility profiles were correlated with magnetic remanence characteristics (natural remanent magnetization, NRM, anhysteretic remanent magnetization, ARM, saturation isothermal remanent magnetization, SIRM, ARM/SIRM, S ratio) determined by the 760-R SQUID Rock Magnetometer (2G Enterprises, magnetic moment $<\!10^{-12}~\mathrm{Am^2}$) complemented with ARM unit and the SI-6 Pulse Magnetizer (Sapphire Instruments) capable of 1100 mT peak induction. Later during the research project, the magnetic remanence was

measured using the JR-6 spinner magnetometer (AGICO Ltd., sensitivity 2×10^{-6} A/m). The AGICO Ltd. LDA-1 demagnetizer complemented with AMU-ARM unit was used to impart an ARM to the samples. A MMPM10 Pulse Magnetizer (generating magnetic field up to 3 T) was applied to induce the IRM in the sediments. While NRM and SIRM are, for samples of the same composition, sensitive to the concentration and grain size of magnetic minerals, ARM is controlled by the relative content of fine-grained (sub-micron) stable single-domain (not superparamagnetic) magnetite (see, e.g., Peters and Dekkers, 2003). The S ratio

(S = (1 - IRM $_{-300~mT}/SIRM)/2$, after Bloemendal et al., 1992) reflects the composition in terms of ferrimagnetic magnetite/maghemite and antiferromagnetic hematite/goethite. SIRM of magnetically soft magnetite is completely remagnetized after application of 300 mT in the opposite direction, while hematite practically retains the original value and direction of SIRM. Thus, S ratio for magnetite would be 1, while low S ratio values indicate higher relative contribution of hematite.

Magnetic hysteresis parameters of the bulk sediments or magnetic extracts were acquired using the MicroMag VSM (Princeton Measurements Vibrating Sample Magnetometer) in magnetic field ranging between $-1.8\,$ and $1.8\,$ T (sensitivity $5^{-9}\,$ Am²). A paramagnetic contribution (high-field magnetic susceptibility) was calculated from the acquired hysteresis loops as a slope of the linear part at fields above saturation of the ferrimagnetic component (typically above 1 T). This was then subtracted from total mass-specific susceptibility in order to assess the susceptibility related to ferrimagnetic component only, assuming that the paramagnetic component is the same for low and high field region. The same device equipped with an Edwards High Vacuum System was used for thermal demagnetization of magnetic extracts to determine the Curie points of the remanence carrying minerals.

Sediment grain size measurements were performed using Fisher MICROTRAC II laser granulometer after a treatment of sediment specimens in the ultrasonic liquid homogenizer. The grain-size values are expressed as an average of the measured data set. Mineral magnetic particles were separated using a permanent magnet applied on the floodplain suspended sediments. In order to preform micro-chemical analyses, magnetic extracts were cast in a resin and polished. The analyses were conducted using a scanning electron microscope (SEM) VEGA 3XM (Tescan, Czechia) with the multi-purpose Quantax 200 system (Bruker, Germany). The energy dispersive spectrometry (EDS) was carried out in high-vacuum mode, accelerating voltage of 20 kV, absorbed by the stream of 500 pA, spot size of 0.5 μ m, and working distance for the analysis of 15 mm. The SEM images were obtained using a back-scattered electrons detector.

The magnetic measurements and experiments were performed at the Laboratory of Environmental Magnetism and Paleomagnetism at Michigan Technological University in Houghton, at the Institute for Rock Magnetism at University of Minnesota in Minneapolis, in the Paleomagnetic Laboratory of the Institute of Geology CAS in Prague, and in the laboratory of Rock Magnetism of the Institute of Geophysics CAS in Prague. The SEM analyses were accomplished at the Institute of Geology CAS in Prague.

3.2.2. Radiocarbon dating

Samples of wood (with weight 10–20 g) collected from the studied sections were processed for radiometric method of 14 C analysis in the CRL radiocarbon laboratory of the Nuclear Physics Institute CAS v.v.i. during period 2006–2011, using acido/alkali/acid pretreatment, combustion and benzene synthesis, Gupta and Polach (1985). The resulting benzene samples were measured with a Quantulus 1220, low-background liquid scintillation spectrometer. Standard Reference Material Oxalic Acid II (NIST SRM 4990C) was used for calibration of liquid scintillation counting. Radiocarbon age in years BP was calculated following the Stuiver-Polach convention (Stuiver and Polach, 1977) with associated combined uncertainty (1σ) according Curie to (1995). Tiny charcoal samples were dated in the Poznań Radiocarbon

Laboratory in Poland (Poz) using acido/alkali/acid pretreatment, combustion and hydrogen based routine of graphitization (Czernik and Goslar, 2001). No freshwater fossils were found in the collected material.

The conventional radiocarbon ages and corresponding uncertainties were subsequently converted into the intervals of calibrated age using OxCal 4.4 software with radiocarbon calibration curve IntCal20 (Ramsey and Lee, 2013; Ramsey, 2009; Reimer et al., 2020).

3.2.3. Dendrochronological dating

Samples of subfossil oak-tree trunks were taken in the form of discs using a chainsaw. The analysis was performed in correspondence with the standard dendrochronological methodology (Cook and Kairiūkštis, 1990). The tree-ring thickness was measured using a VIAS TimeTable measuring system. Measuring and synchronizing of tree-ring series was carried out using the PAST4 (OSciem) application. The annual wood increments were measured with 0.01-mm accuracy. The growth trend of individual tree-ring series was removed by the ARSTAN application (Grissino-Mayer et al., 1992) using a two-step standardization method (Holmes et al., 1986). First, a negative exponential function or a linear regression curve, the one which best expresses the change of the growth trend with age, were used (Fritts et al., 1969). Other potentially non-climatically conditioned fluctuations of values of radial increments, brought about by, e.g., competition or forester's interference, were balanced using the cubic spline function (Cook and Peters, 1981). The chosen length of the spline function was 32 years (Cook and Kairiūkštis, 1990). Then the individual tree-ring series were cross-dated. The cross dating is a search for the synchronous positions of two tree-ring series. The synchronous position is demonstrated by a sufficiently high similarity in the area where the tree rings overlap (Cook and Kairiūkštis, 1990). The degree of similarity between the tree-ring series was evaluated using the correlation coefficient and the parallelism coefficient (Gleichläufigkeit, Schweingruber, 1983). These calculations facilitate the optical comparison of both series, which is crucial for the final dating (Rybníček et al., 2010). The well correlating series were used to create the average tree-ring series. Three average tree-ring series were dated using the Moravia oak tree-ring chronology MORGES 2010 (Kolář et al., 2012). When the dated series overlaps with the tree-ring chronology by more than 60 tree rings, the critical value of Student's t-distribution at 0.1% level of significance is 3.460 (Smelko and Wolf, 1977). When the samples did not contain sapwood tree rings, we could only ascertain the year after which the trees fell. Based on empirical studies, the oak sapwood usually contains at least 5 tree rings related to the tree age and location in the Czech Republic (Rybníček et al., 2006; Prokop et al., 2017). These tree rings need to be added to the interpreted age.

3.2.4. Deposition age estimation based on 137 Cs activity and persistent organic pollutant (POP) content

The 137Cs analyses were performed to estimate the depositional age using the identification of the most recent pollution associated with atomic bomb testing and the Chernobyl nuclear power plant accident. Sediment samples were dried (105 $^{\circ}$ C) and sieved through a 2 mm mesh. Gamma spectrometry was performed utilizing a HPGe detector with a relative counting efficiency of ca. 20% and 1.8 keV energy resolution (on 1170 keV from ⁶⁰Co). Specific activities of ¹³⁷Cs were decay-corrected to date 16.5.2006, when sediments were sampled. The corresponding combined uncertainties were calculated for 1σ following Curie (1995). The analyses were performed in the CRL radiocarbon laboratory of the Nuclear Physics Institute CAS v.v.i., Prague (Czechia). Despite the fact that the $^{137}\mathrm{Cs}$ and $^{210}\mathrm{Pb}$ dating cover approximately the same age of last hundred years and may be cross-correlated, in this study we used only the former dating method. The main aim was to see the effect of the Chernobyl event in 1986. The latter method was used in Kadlec et al. (2009), but cross-correlation of the ages is beyond the scope of yhis study.

The concentrations of dichlorodiphenyltrichloroethane (DDT) and polychlorinated biphenyl (PCB) were determined using Varian GC 450

gas chromatograph in the VZ Lab Ltd., Prague (Czechia), whereas the total carbon content in the floodplain deposits was analyzed using TOC Shimadzu device (model TOC-VCPN) completed with ultra-red detector NDIR at the Czech Geological Survey, Prague (Czechia).

3.2.5. Timing of the flood events based on correlation of point bar sediment lithology and historical flood record

The modern point bar bodies have been formed in the canalized segments of the Morava R. since the late 1930s. Starting from the point bar top in the Section S8 (Fig. 1), we followed the lithological changes represented by sandy and clayey couples deposited during a single flood event. Number of the couples was compared with a bank-full discharge record archived by the Czech Hydrometeorological Institute in Brno.

4. Results

4.1. Lithologies and architecture of the floodplain deposits

On the basis of the sedimentary character and dating of preserved organic material, the floodplain sequences exposed along the Morava River can be divided into 5 distinct units (Fig. 2). The oldest Unit 1 is composed of grev medium to coarse-grained sands and sandy gravels directly deposited in an ancient river channel of the Morava River. Interbedded with these sands and gravels are thick lenses (up to 50 cm) of dark organic fen-like sediment, that also contain tree-trunk and wood fragments. Unit 2, which overlies Unit 1, consists of greyish clayey silt to silty clay deposited in an overbank environment. This unit has thickness of up to 200 cm and contains a basal horizon composed of plant roots. The next younger unit (Unit 3) consists of grey channel sands and gravels. The thickness of this unit is up to 330 cm and contains tree fragments (mainly oak); rare freshwater mollusk shells are also found near the base of this unit. In two sections of Unit 3, tree trunk relics showing in situ growth positions were identified. In addition, several wooden poles, pegged to the underlying deposits of Unit 2, were exposed in Section S9 due to modern river erosion. Lastly, the base of Unit 3 also contains plant roots including reed-mace roots. Unit 4 overlies Unit 3 and consists of greenish, light grey or whitened overbank sandy clay or clayey sand and brown or greenish massive clayey to sandy silt reaching up to 190 cm in thickness. The base of the unit often contains a soil horizon and plant roots. Reductimorphic Fe-oxide stains or ferric rhizoliths dominate this unit. Charcoal horizons are also common. The upper parts of this unit contain cut and fill structures associated with Unit 5. The Unit 5, up to 200 cm thick, is formed by brownish sandy or clayey silts, intercalated with lenses or sand layers up to 20 cm thick, representing a natural levee or crevasse splay deposits, respectively. The sediments contain charcoals and scarce wooden fragments close the base of the unit. The top of the Unit 5 is covered by modern vegetation.

Point bar deposits, which have been formed recently in the canalized passages of the meandering river channel, show alternating beds of light brown sand and dark brown clayey silt with thickness varying between 2 and 55 cm. The total thickness of the point bar sequences, exposed above the water level, can reach up to 400 cm.

We also drilled through the organic deposits, filling one of abundant meander channels at the floodplain edge (Sections S15 and S16). The obtained core consists of 194 cm thick dark fen-like deposits (mostly gyttja) intercalated by river channel sand 106 cm thick.

4.2. The age of the floodplain deposits

Radiocarbon dating of the organic materials preserved in situ in various units, i.e. the tree-trunk fragments standing vertically in the sediments, reed-mace roots, wooden piles pegged in the clayey sediments and fixed with stones, were compared with dendrochronological ages of the oak-tree trunks buried in the floodplain deposits. The tree-ring thickness variations enable to determine three series with end times of 1058, 1322, and 1647 years AD. Statistical similarity between

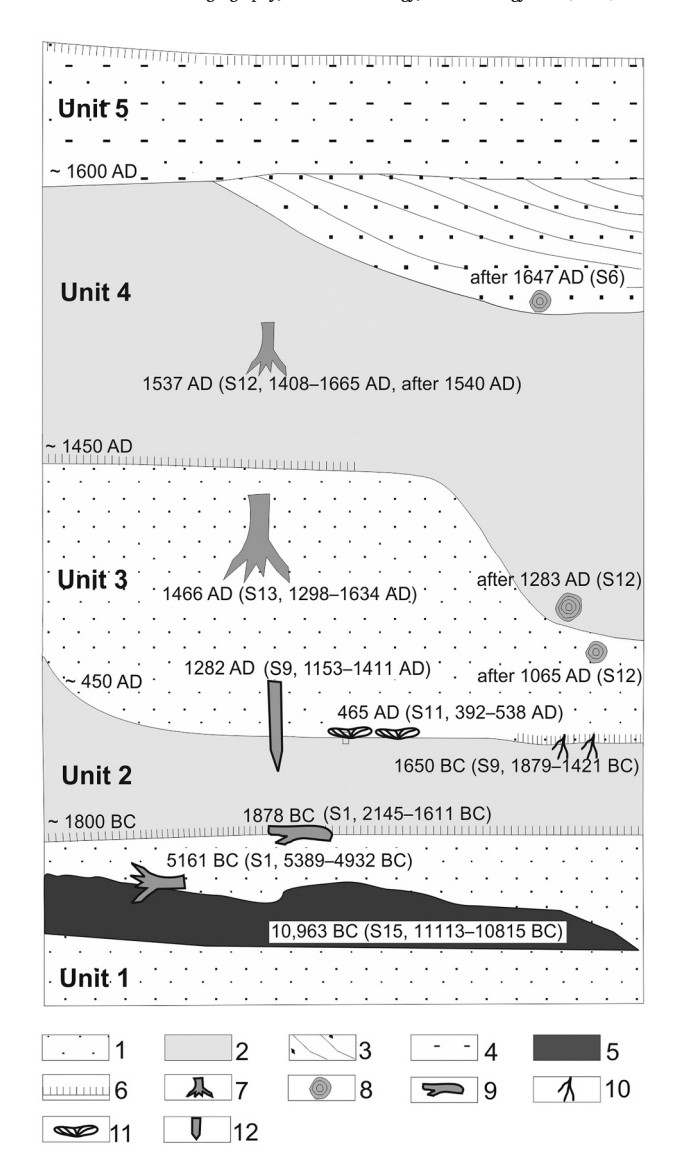


Fig. 2. Scheme of floodplain sequences (not to the scale) based on sediment lithology and dating of preserved organic material. Radiocarbon ages are shown as calendar years by a median of two-sigma time interval (in parentheses, see Table S1 in Supplementary file).

1 – Meandering channel sand and sandy gravel, 2 – Overbank silty and clayey deposits, 3 – Point bar sandy and silty deposits, 4 – Natural levees sandy and silty deposit, 5 – Organic sediments, 6 – Soil horizon abundant with vegetation roots, 7 – Tree trunks in situ position, 8 – Re-deposited tree trunks, 9 – Wood fragments, 10 – Reed-mace roots, 11 – Mollusk shells, 12 – Cut pole pegged into sediments

the average series and the tree-ring chronology is very high. Also calculated *t*-test values are considerably high, supporting good reliability of dating results. All obtained ages are summarized in the Table S1 (Supplementary file).

The oldest floodplain deposits (Unit 1) are preserved in the fossil meanders at the NW floodplain edge (Sections S15 and S16). The basal organic sediments were deposited during Late Glacial as indicated by the age of the gyttja dated to 10,963 (11113–10,815) years BC. The organic-rich sediments corresponding with the Unit 1, preserved at a base of the Section S1, revealed an age of 8921 (9141–8701) years BC, whereas the wood and tree-trunk fragments from the same unit span time interval between 5398 and 1611 years BC (Kadlec et al., 2009).

The overlaying overbank deposits (the Unit 2) were deposited after ca. 1800 years BC and they were partly destroyed by lateral erosion since ca. 450 years AD. The Unit 3 covers time span between ca. 450 and 1450 years AD. The age of the overlaying overbank deposits of the Unit 4 varies between ca. 1450 and 1600 years AD and the youngest Unit 5 has been depositing since 1600 years AD based on radiocarbon and dendrochronological dates (Table S1 in Supplementary file, Fig. 2).

The increased ¹³⁷Cs activities, corresponding to contamination related to the Chernobyl nuclear accident in 1986 and nuclear weapons test (namely in beginning of 1960s), are detectable down to 90 cm below the floodplain surface in the sediments exposed in modern point bar sediments (Section S8). However, in the more distant floodplain sediments the measurable ¹³⁷Cs concentrations were detected only in the topmost 25 cm of the sequences (Fig. 3). The ¹³⁷Cs-related peak also proves that this sediment layer was deposited after the flood dykes construction.

Increased POP (DDT) concentrations are present in the topmost portion of the floodplain sequences. The contamination extends to 35 cm below the floodplain surface (between the dykes) and 10 cm below the present-day floodplain surface (outside the dykes), respectively (Fig. 3).

4.3. Mineral magnetic characteristics

4.3.1. Magnetic susceptibility

The mass-specific low-field magnetic susceptibility (χ) determined in the river-side sections reaches the highest values (30 to 48 \times $10^{-8} \text{m}^3 \text{kg}^{-1}$) in the topmost 30–50 cm in each section (Figs. 4–6). The χ values then show a noticeable decrease downward to 200 cm depth and remain low throughout the rest of the sections. The deepest parts of our sections show χ values of about 10×10 –8 m3/kg and lower, which correspond well with the values of the deepst layers from the same area in Grygar et al. (2010, 2011). Occasionally there are some local peaks between the magnetically enhanced topmost layer and the depth of about 200 cm. Only the topmost ~25 cm of the floodplain sequence (Unit 5) reveal reliable values of the frequency-dependent magnetic susceptibility χ fd%, usually between 2% and 4%, occasionally reaching

7% (Fig. 4). Values of 4% and higher may indicate presence of nanosized superparamagnetic magnetite of pedogenic origin (Dearing et al., 1996). Below 50 cm, this parameter shows very scattered, and even negative values (not justified by physics), which are considered as artefacts due to low sensitivity of the instrument (volume susceptibility being well below 10×10^{-5} a.u.). The other sections show similar behavior.

The modern point bar deposits (Section S8) show variations χ below $20 \times 10^{-8} m^3 kg^{-1}$ in the topmost 90 cm. The middle portion of the section reveals higher oscillations up to $60 \times 10^{-8} m^3 kg^{-1}$, with susceptibility peak values related to the finer deposits. The exposed lower part of the point bar shows susceptibility variations around $20 \times 10^{-8} m^3 kg^{-1}$ (Fig. 7).

Vertical distribution of magnetic susceptibility in two neighboring sections, separated by flood dyke, is shown in Fig. 8. The floodplain sediments deposited outside the dyke do not record any remarkable magnetic enhancement in the topmost portion of the sedimentary sequence. The mass-specific magnetic susceptibility curve is practically flat with values oscillating between 6.1 and $10.1 \times 10^{-8} \mathrm{m}^3 \mathrm{kg}^{-1}$. This more or less stable pattern can be observed also in the deeper part (below 50 cm) of a neighboring section inside the flood dyke (Fig. 8). The change in the pattern in depth of about 50 cm may reflect the effect of higher erosion rate combined with the protective role of the flood dyke. However, this observation does not have general validity; sections more distant from the dyke show different patterns.

There is no meaningful correlation between vertical distribution of χ and the sediment mean grain size (Fig. 9, Pearson correlation coefficient R of -0.0525 for Section S1 and 0.138 for Section S12). Available age data do not enable reliable interpretation of the anomalies. Probably, the peak in grain size in Section S12 may be linked rather to formation of modern meander belt around 1650 than to the beginning of the Little Ice Age. Heating curves of the temperature dependence of (volume-specific) magnetic susceptibility κ show changes of magnetic phases with increasing temperature (Figs. S1 and S2 in Supplementary file). The first

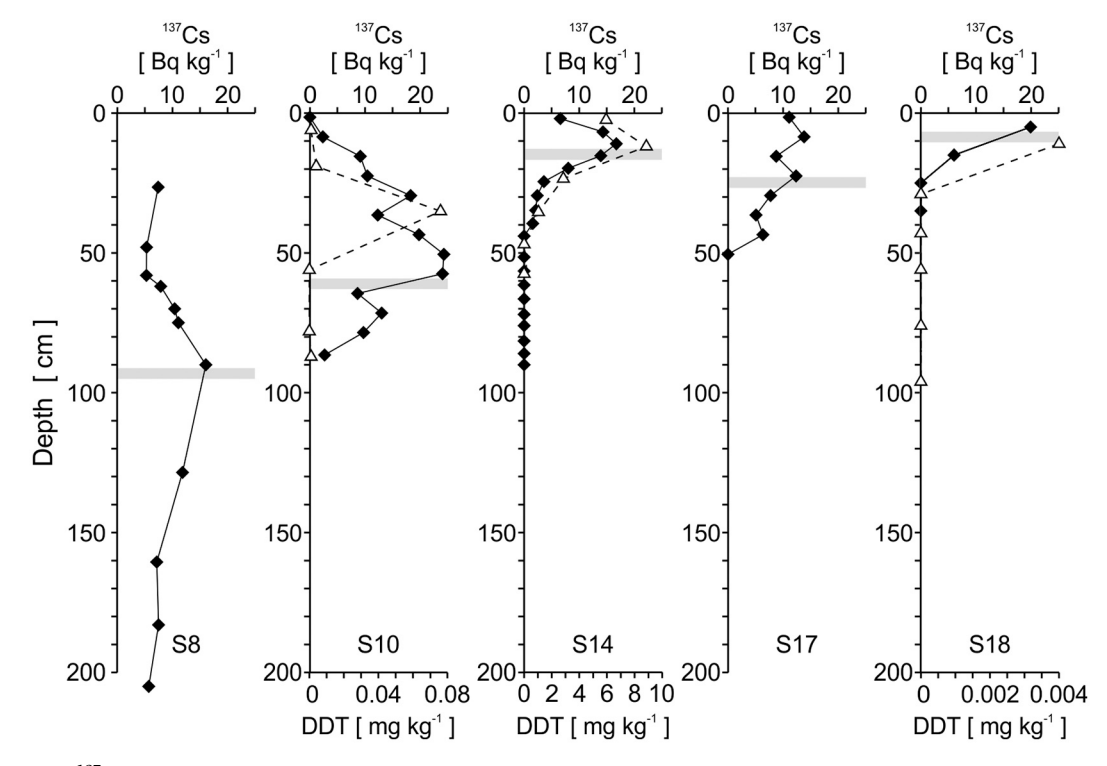


Fig. 3. Variations of the ¹³⁷Cs activity (full symbols) and dichlorodiphenyltrichloroethane (DDT) dry-mass concentration (open symbols) along the selected sections. Grey bands indicate horizons corresponding to the Chernobyl nuclear accident.

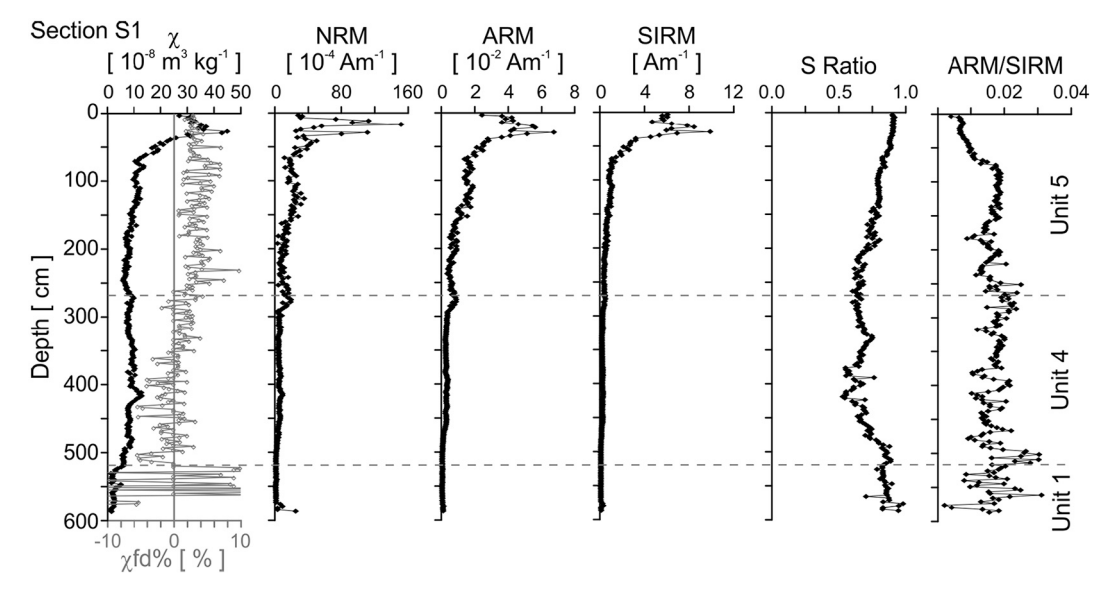


Fig. 4. Magnetic mineral characteristics along Section S1. χ – low-field mass-specific magnetic susceptibility, χ fd% – frequency-dependent susceptibility (anomalous values out of range not shown), NRM – natural remanent magnetization, ARM – anhysteretic remanent magnetization, SIRM – saturation isothermal remanent magnetization.

increase at 270–300 °C is followed by κ decrease. This can be attributed to the presence of organic carbon (Maher, 1998; Kapička et al., 2001, 2003), rather than to the presence of iron sulphides (such as antiferromagnetic greigite). Next increase peaks at about 500 °C, and is followed by steep decrease usually to values close to zero. Curie point is estimated to be between 550 and 580 °C, using the linear paramagnetic behavior of inverse susceptibility (Petrovský and Kapička, 2006; Fabian et al., 2013). This suggests the presence of magnetite. The changes in magnetic phases are more distinct with increasing organic matter content in the sediments (Fig. S1 in Supplementary file). The cooling curves reach higher values due to magnetic phase changes in the sediments. The changes are more distinct in the fine sediment fraction below 0.5 mm (Fig. S2 in Supplementary file).

4.3.2. Remanent magnetizations

The NRM, ARM, and SIRM records show similar patterns. The highest values occur in the topmost ca. 50 cm in the sections, followed by decrease downward through occasional local maxima in the sections to 200 cm depth, and then stay very low throughout the rest of the sections (Figs. 4–6). Variations of the S ratio show decrease in the clayey bed whereas the ARM/SIRM values are decreasing in the bottom portion of the sections, followed by slight rise in the clayey sediments and a decrease in the upper portion of the sections.

The presence of magnetite in the upper ca. 50 cm of the studied floodplain sequences is documented by the Curie temperature (578 $^{\circ}$ C) revealed by temperature dependence of remanent magnetization, measured from room temperature to 700 $^{\circ}$ C on magnetic extracts from

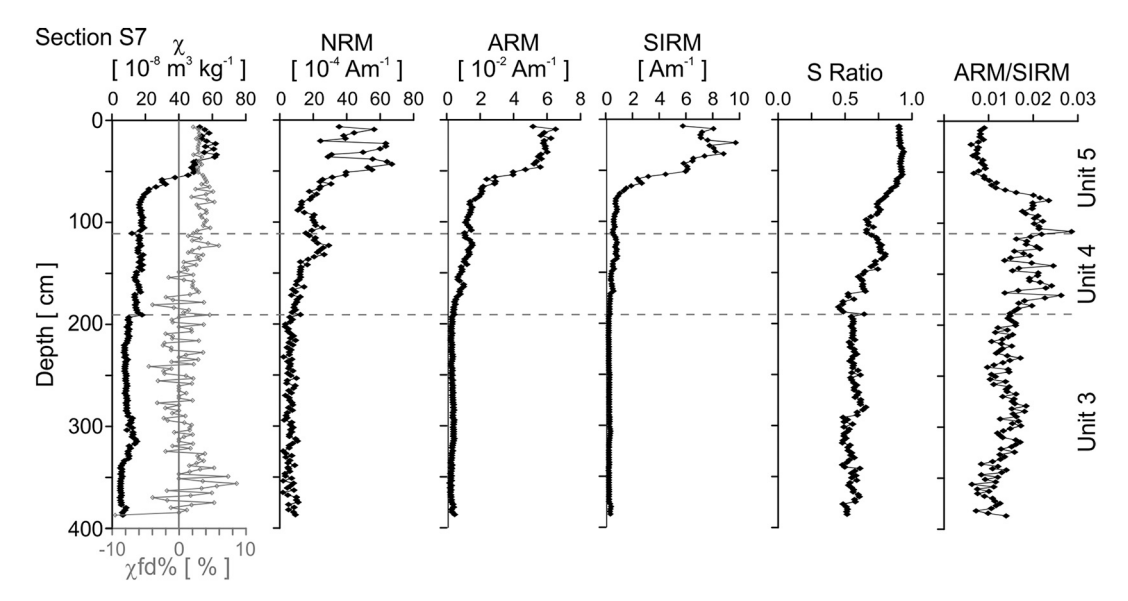


Fig. 5. The same as in Fig. 4, but for Section S7.

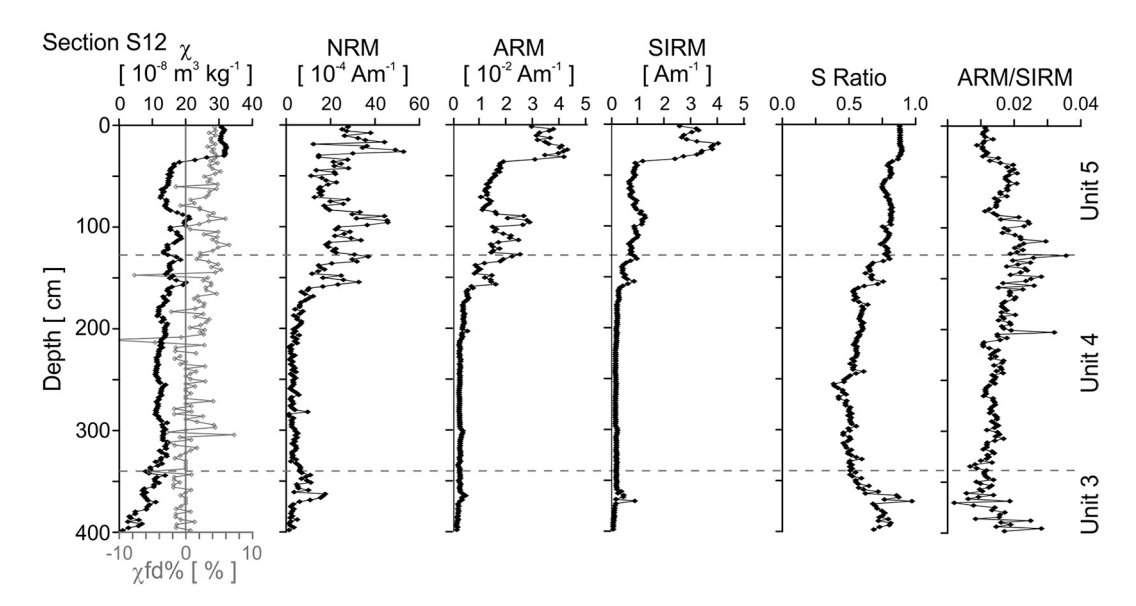


Fig. 6. The same as in Fig. 4, but for Section S12.

the horizon 32.8 cm in the Section S12 using MicroMag VSM (not shown). The presence of low-temperature oxidized magnetite (Özdemir et al., 1993) is also supported by weak Verwey transition at about 120 K, observed on curves of temperature dependence of remanent magnetization acquired at room temperature in the field of 2.5 T and measured from room temperature down to 5 K for both bulk specimen and magnetic extract of the same horizon using MicroMag VSM (not shown). The same ordering related to the Verwey transition was reported by a susceptibility increase at about 120 K (Kadlec and Diehl, 2005). The IRM/SIRM ratios show a presence of magnetically "weaker" mineral in the topmost part of the floodplain sequences following increased concentration of magnetically "harder" minerals downward (mainly in the Unit 4) in the Sections S1, S7, and S12 (Figs. 4–6).

The NRM, ARM, SIRM variations, measured in the modern point bar deposits are related to the sediment lithology changes. The higher values were mostly measured in the clayey layers whereas sandy beds show lower signal of the remanent magnetizations (Fig. 7).

4.3.3. Magnetic hysteresis

The low and high temperature VSM experiments yielded very narrow hysteresis loops. The magnetic saturation of measured sedimentary material is low especially in the lower portions of the sections (Figs. S3 and S4). Shape of the loops is typical for ferrimagnets. In deeper layers, the loops are practically straight and reversible, suggesting prevalence of paramagnets. Antiferromagnetic phases such as hematite or greigite would, in mixture with magnetite, result in wasp-waisted loops (e.g., Tauxe et al., 1996), which we did not observe. The peak observed on thermomagnetic curves at 270–300 °C (Figs. S1 and S2 in Supplementary file) may suggest the presence of goethite, but it is rather the effect of organic carbon, observed in humus-rich topsoils (e.g., Maher, 1998;

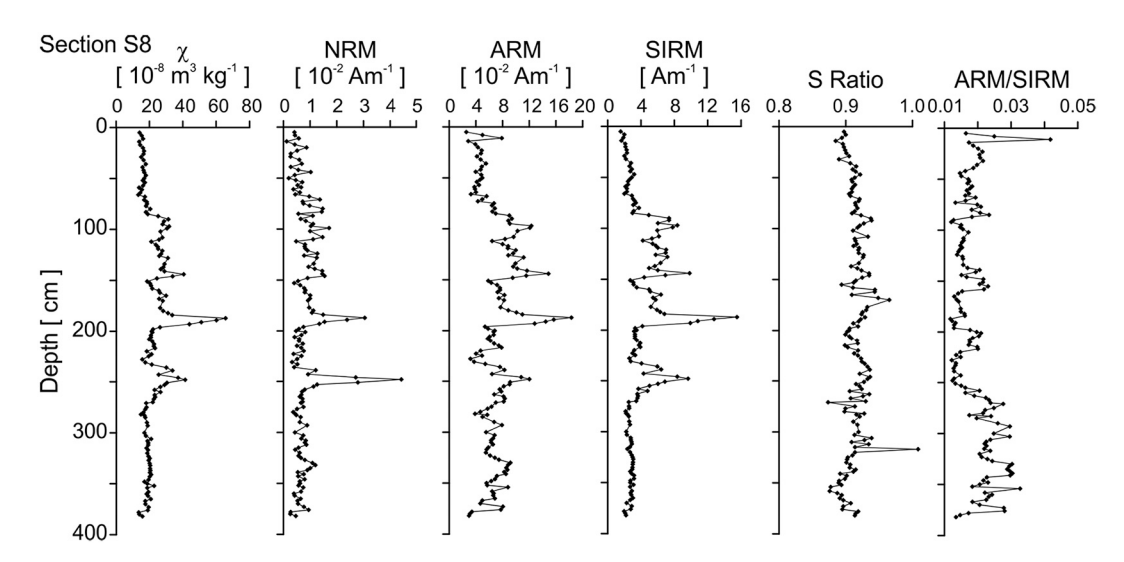


Fig. 7. The same as in Fig. 4, but for Section S8 (point bar). Drop of susceptibility at about 90 cm corresponds to the Chernobyl event in 1986 (Fig. 3).

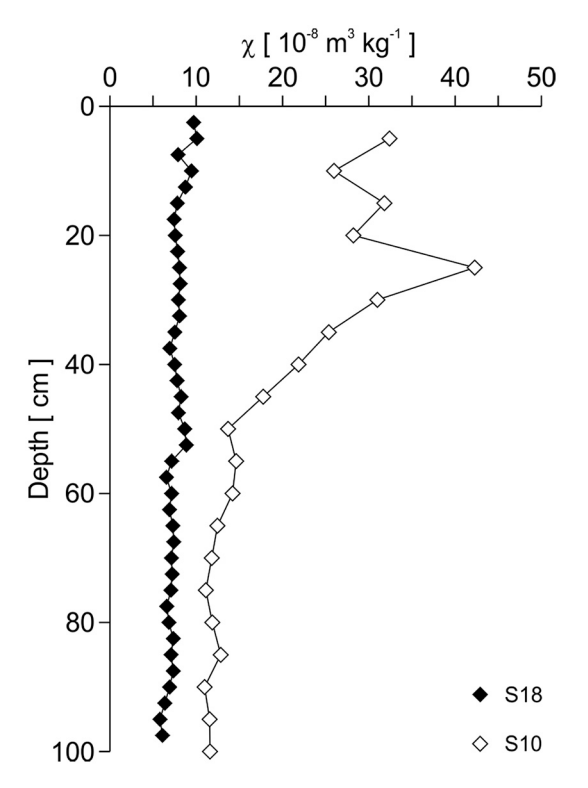


Fig. 8. Mass-specific magnetic susceptibility χ of the floodplain sediments outside (Section S18) and inside (Section S10) the flood dykes.

Kapička et al., 2001, 2003). Magnetite contents in the Section S12, calculated from the saturation magnetization, assuming the value of 92 $\rm Am^2/kg$ for pure magnetite (e.g., Dunlop and Özdemir, 1997), vary between 0.013 and 0.236% in the uppermost 150 cm of the sequence and between 0.003 and 0.01% below 150 cm.

The high-field susceptibility values reach 3 to $10 \times 10^{-8} \, \text{m}^3 \text{kg}^{-1}$ and generally correlate with the mass specific susceptibility variations. The percentage ferrimagnetic component χ_{ferri} of the total susceptibility, calculated using χ_{low} , χ_{high} , and χ_{total} values, is increasing upwards in the section, except for the sandy layers (Fig. 10).

4.3.4. Scanning electron microscope analyses

The SEM images of the magnetic extracts show both spherical and angular particles of sizes up to 100 μm . Composition of the spherical particles is varying from dominating FeO to mixture of FeO and SiO $_2$ or FeO and TiO $_2$ (Table S2 in Supplementary file). Some of the microchemical analyses revealed increased Al $_2$ O $_3$ concentration. Angular particles are composed of FeO or a mixture of SiO $_2$ and FeO, including higher content of MgO, Al $_2$ O $_3$ or CaO (Table S2 in Supplementary file). Spherical magnetic particles were found in the topmost 50 cm of the floodplain sequences. However, they are missing below this depth,

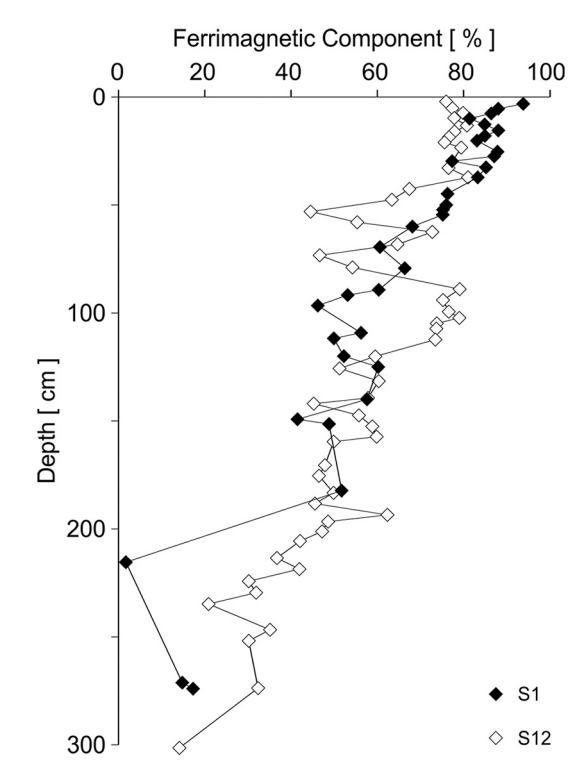


Fig. 10. Ferrimagnetic component variations through the floodplain sequences (Units 4 and 5) exposed in the Sections S1 (upstream) and S12 (downstream).

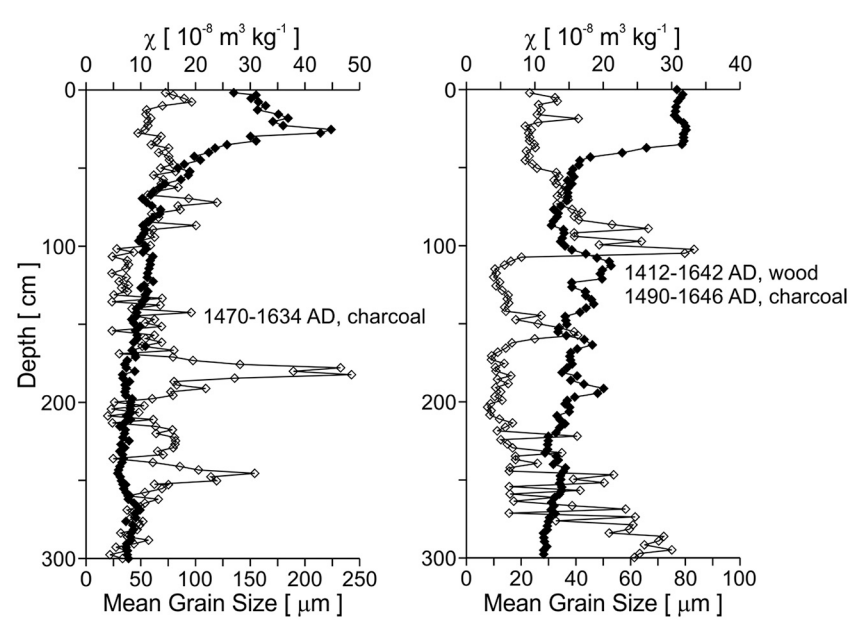
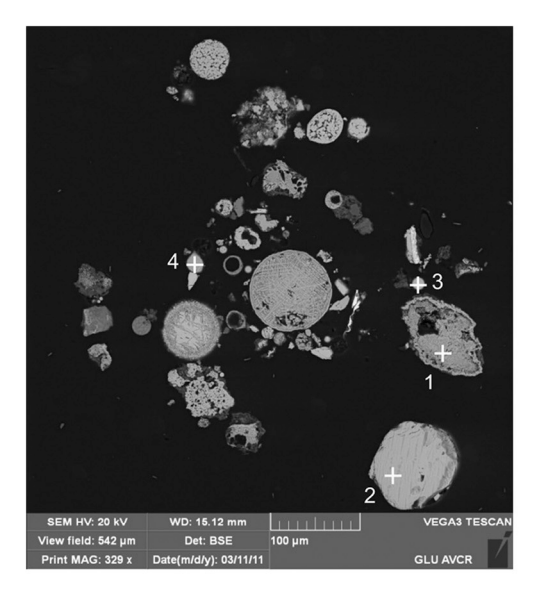
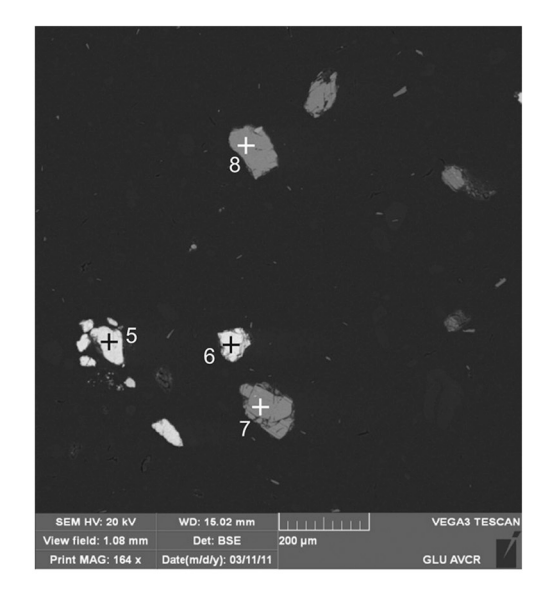
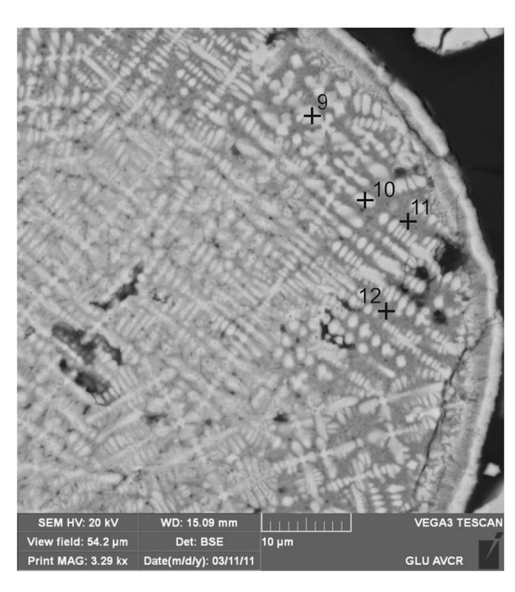


Fig. 9. Comparison of mass-specific magnetic susceptibility χ (full symbols) and sediment mean grain size (open symbols) in the Section S1 (left) and S12 (right).







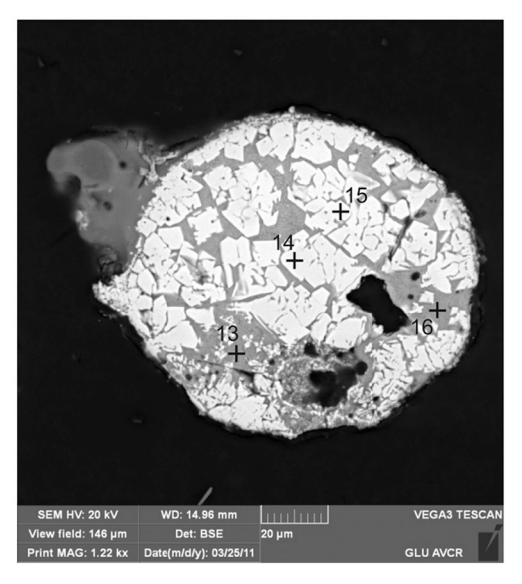


Fig. 11. The SEM images of the magnetic particles present in the magnetic extracts acquired from the floodplain deposits exposed in the Sections S10 and S17. Top left – natural angular and industrial spherical magnetic particles from 5 cm depth, Section S10; top right – natural angular magnetic particles from 100 cm depth below present-day floodplain surface, Section S10; bottom left – detail of the spherical particle from the center of the image at top left; bottom right – detail of the spherical particle from the depth 7 cm, Section S17. For chemical composition of the particles see Table S2 (Supplementary file).

where only angular magnetic particles are present (Fig. 11).

5. Discussion

5.1. Timing of the fluvial processes

The Morava R. floodplain sediments were deposited in channel and/ or overbanks related to the meandering river. Using combination of lithological assessment and several dating approaches we were able to determine a succession of up to five periods of the floodplain sediment aggradation (Units 1-5) – see Fig. 2. However, not all the units are preserved in one complete section. Modern river side exposures usually show only the younger sedimentary Units 3-5.

The oldest floodplain organic deposits (Unit 1) were found in palaeomeander relics at the NW edge of the Morava R. floodplain (Section S15). These sediments were deposited during the late deglacial period or early Holocene (11158–10,771 years BC). In contrast, the channel sand and sandy gravels, also from Unit 1, but exposed at the

base of the Section S1, contain organic deposits including wood and tree trunk fragments yielding ages between 9150 and 1602 years BC (using radiocarbon dating, Kadlec et al., 2009). Large scatter of ages acquired from this single sedimentary bed is a result of complete reworking of older floodplain deposits by the river channel lateral shift, causing a concentration of tree fragments of different age in one layer (see Kalicki and Krapiec, 1995). Unit 1 deposits were overlain by clayey overbank sediments of the Unit 2. Dating of reed-mace roots from the upper part of this unit yielded an age of 1650 (1879-1421) years BC. Angular cut poles, forming possible part of a foot bridge, were pegged into that clay surface of the Unit 2 in the Section S9. Age of the poles is 1282 (1153-1411) years AD (Kadlec et al., 2009). Radiocarbon dating of shells, in situ preserved stump, and the dendrochronological dating of the tree trunk fragments show that the Unit 3 was deposited between ca. 450 and 1450 AD. During the same period, the fluvial sand and sandy gravel completely filled the meandering several meters deep river channels surrounding the archaeological complex of the Mikulčice Castle located 20 km downstream. The channels were used for fishing

and boat transportation during the 9th/10th century, when the castle was the most flourishing (Poláček, 2000). Especially the first half of 14th century was affected by extreme floods (e.g., Brázdil et al., 2011a, 2011b) and running water erosion due to heavy rains combined with extended central European agriculture activities. The most devastating flood in last 1500 years occurred in the central Europe in 1342 (Bork, 1989)

Unit 4 in the Morava R. floodplain sequences spans time period between 1450 and 1650 AD based on radiocarbon dating of the charcoal and wood fragments. The dendrochronological age of the tree trunk fragments, preserved in the Section S6, revealed the meandering channels incision into the under laying Unit 3 and subsequent filling since 1650 AD (Fig. 2). The age of the youngest Unit 5 covers time interval since 1650 AD until present. The topmost portion of the floodplain sequences, up to 70 cm thick, was deposited after the last mid-century based on the POP (DDT) and ¹³⁷Cs age estimation (Fig. 3). The ¹³⁷Cs contamination, preferentially fixed to silty and clayey particles, partly migrated vertically downwards due to groundwater level oscillations. Therefore the measured ¹³⁷Cs activity decreases continuously bellow the interpreted Chernobyl nuclear accident marker (see Sedláček et al., ²⁰¹³)

The modern point bar bodies have been formed by sediment accretion during flood events when the Morava R. discharge exceeds 470 $\rm m^3 s^{-1}$ (Pilařová, 2008). The single flood creates a couple of sandy and silty layers (Fig. 7). Correlation of these couples with measured discharge record allows us to assign the sediments to discrete flood. This approach was supported by the $^{137}\rm{Cs}$ activity measured in the sediments. The highest $^{137}\rm{Cs}$ values, related to the 1986 year, was detected 90 cm below the top of the point bar (Fig. 3). This may be related to drop in susceptibility observed in Section S8 (Fig. 7). This is consistent with the flood records referring to about 7 floods since 1986 (Pilařová, 2008). Thus, it seems that point bars, e.g. Section S8 (Fig. 7), reflect better flood events than floodplain sediments. However, to prove this, more reliable dating values should be available.

We are not able to estimate the average aggradation rate for Units 1 and 2. The Unit 1 represents time period since Late Glacial to the end of the Mid- Holocene climatic optimum. Following climatic deterioration, erosion and complete reworking of the older floodplain fills by meandering river channel occurred. Thickness of the above lying overbank deposits (Unit 2) was most probably also modified due to partial erosion. Therefore, the sections along the erosional river banks usually show only the younger portion of the Morava R. floodplain fill (Units 3-5). The channel sand and sandy gravel (Unit 3) reflect increased fluvial activity since the 9th and especially in the 10th century, as documented in the fluvial systems across central Europe (Kalicki, 2006). We can estimate an average aggradation rate of about 0.2 cm/year in the Unit 3. The average aggradation rate in the above laying overbank clayey deposits (Unit 4) rises to 1.2 cm/year probably due to increased erosion of soils related to the field land enlargement and Medieval agriculture climax in the Morava R. catchment (see Svoboda et al., 2003). The forest clearance and intense burning are documented by charcoal horizons abundant in the Unit 4.

Formation of modern meander belt (about 1650 AD, early period of the Unit 5) was triggered by climatic deterioration in the Little Ice Age, and is continuing until present. The floodplain deposition along the modern river channel was accelerated since the flood dykes construction in the late 1930's. Formation of extremely large agricultural fields since 1950's also contributed to the soil erosion enhancement (Zádorová et al., 2011). The average aggradation rate ranges between 0.7 and 1 cm/year during the last 70 years. The depositional rates assumed by Grygar et al. (2011), based on geochemical logging in the Morava R. floodplain, seem to be underestimated probably due to uncertain timing of the depositional events. Use of radiocarbon dating of possibly older re-deposited organic material (charcoal and small tree branch fragments) to the younger floodplain sediments could complicate final interpretation of the depositional history.

5.2. Natural factors controlling the mineral magnetic variations in the floodplain deposits

The magnetic properties of the source material and post-depositional weathering and pedogenic processes, both in the floodplain and in the catchment area, are the main factors controlling the resulting magnetic characteristics of the floodplain deposits. The soils, developed during the Holocene on glacial loess or loess-derived deposits in the Morava R. catchment, represent the main source of magnetic minerals transported and deposited in the floodplain environment. The lithology and diagenetic grain size variations of the floodplain sediments play also a crucial role and complicates the use of the mineral magnetic techniques. Our data suggest that only Unit 5 (at some places may be also Unit 4) preserves original magnetic particles, which did not undergo diagenesis through gleying, and is thus the most suitable for the magnetic analyses. For this reason, in the Strážnické Pomoraví floodplain area, the sediments available for mineral magnetic study cover time interval of ca. last 600 years. However, the groundwater oscillation in the floodplain deposits accelerated the post-depositional reductive dissolution of iron oxides caused by gleying processes (e.g. Thompson and Oldfield, 1986), which erased the magnetic signal from depths 250–300 cm downwards. The ferrimagnetic minerals were replaced by goethite as documented by low temperature demagnetizing experiments and decreased S ratio (Figs. 4–6). The presence of goethite in most of the investigated sections, together with a significant paramagnetic contribution, made it impossible to interpret meaningfully the Day plot (Day et al., 1977) from our VSM data. The applicable magnetic record is thus reduced to about the last 400 years.

The reductive dissolution of ferrimagnetic carriers decreased χ and magnetic remanence values in the lower portion of the Unit 4. This is followed by a slight increase in the same unit upwards due to higher concentration of the ferrimagnetic minerals (Figs. 4–6). This is most probably related to more intense erosion and re-deposition of the soil particles from the river catchment (Dearing et al., 1987). The increase of both susceptibility and remanence values continues through the above lying natural levee deposits (Unit 5), reaching the highest values in the topmost 50 cm (Figs. 4–6, also discussed later in Section 5.3). Little Ice Age (1450–1850) is known to cause climatic deterioration, accompanied by heavy precipitation, subsequent floods, accelerated field soil erosion and re-deposition of the eroded material in the floodplain (e.g., Rumsby and Macklin, 1996). For instance, Svoboda et al. (2003) reported catastrophic floods and erosion of the arable soil that occurred in the central Europe in periods 1560–1573 and 1576–1582.

Higher values of the SIRM and S ratio in the topmost 50 cm indicate the presence of magnetite with increased magnetic grain size, as suggested by the decrease of ARM/SIRM (Figs. 4–6). Shape of the hysteresis loops also indicates dominating presence of the magnetite. Sandy beds, deposited during floods on the natural levees or in the crevasse splay aprons (Unit 5), are responsible for decrease of the magnetic parameters due to prevalence of diamagnetic quartz grains. In such case, oscillations in magnetic properties are controlled mostly by lithological changes related to the flood water flow regime, depositional conditions and local morphology in the river channel and its surroundings. Therefore, detailed temporal correlations of local maxima and minima in the magnetic logs are difficult.

5.3. Anthropogenic impacts on the mineral magnetic variations in the floodplain deposits

The origin of magnetic enhancement, revealed in the topmost 50 cm of the floodplain sequences, consists of two contributions: (i) magnetite originated during agriculture cultivation of the field soils in the Morava R. catchment, and (ii) magnetic particles related to industrial pollution. While the latter effect is well described in many papers, the former one is less studied. However, land-use processes, such as tillage and fertilizing, increase soil organic matter content, which promotes magnetite

neoformation through soil redox processes (e.g., Frankl et al., 2021). Higher concentration of pedogenic single domain (SD) and/or pseudosingle (PSD) domain particles in the topmost 50 cm of the sediment sequences is supported by the highest ARM values. Presence of magnetite is documented by increased SIRM and higher S ratio values (Fig. 4-6). The uppermost Unit 5 (~25 cm) shows reliable values of the frequency-dependent magnetic susceptibility yfd%, usually between 2% and 4%, occasionally reaching 7% (Figs. 4-6). Values of 4% and higher may indicate presence of nano-sized superparamagnetic magnetite of pedogenic origin (Dearing et al., 1996). Our data suggest that magnetic enhancement is not due to pedogenic SP magnetite. The relatively low concentration of SP particles could be related to their weathering and dissolution during the re-deposition from the fields to the floodplain environment. The upward increasing trends of the ferrimagnetic component in the sedimentary Units 4 and 5 (Fig. 10) document the increase of input of the eroded field soil material to the Morava R. floodplain during last four centuries. This pattern is practically identical for two distant sections, upstream (S1) and downstream (S12), both inside the flood dykes. The erosion is related to agricultural activities along the central segment of the Morava R. since the Medieval times and especially after World War II, when large field tracts were formed during agrarian collectivization since 1950's (e.g., Orsillo, 2008; Pernes, 2016).

The magnetic enhancement, detected only in the floodplain sediments deposited between the flood dykes (Fig. 8), may be attributed to higher accumulation of sediments during high-water events, when the deposition in wider area is prevented by the dam. This may be also affected by incorrect land-use management during the last 70 years during agrarian collectivization, such as merging small fields, removing balks and groves, and monoculture farming, resulting in soil more vulnerable to erosion. Timing of the enhancement correlates with Pb and POP pollution concentrations, increased in the second half of the last century (Kadlec et al., 2009).

The second source of the magnetic enhancement is in the presence of spherical magnetic micro particles, which originated during fossil fuel combustion and consist predominantly of iron oxides or a mixture of iron and silica oxides. Especially magnetite microspherules are formed at high temperatures from pyrite presented in the coal (Flanders, 1994). The magnetic particles were deposited from the air on the Earth surface

and later were re-deposited due to erosion to the Morava R. floodplain. The high concentration of spherical magnetite particles was identified in the depth interval of 0–50 cm below the floodplain surface (Fig. 11), and it reflects increased pollution deposition related to development of the Czechoslovak industry after the World War II. In lower horizons, only the angular magnetic particles were observed in the magnetic extracts (Fig. 11).

The original magnetic signal in older sediments (Units 1, 2 and 3) could be originally higher then today, but has decreased due to magnetic mineral weathering triggered by groundwater oscillation, supporting the gleying processes. Although it is reported that reductive dissolution of, e.g., goethite results in formation of magnetite (e.g., Till and Nowaczyk, 2018), we believe that in our case reductive conditions induced dissolution of the ferrimagnetic minerals, process similar to that described by Sundman et al. (2017), and neoformation of goethite in the clayey beds. The observed magnetic enhancement in the top lavers reflects present distribution of ferrimagnetic iron oxides. The potentially higher values in the older units can't be reconstructed. Therefore, historical record of magnetic enhancement with possibly higher values of the bottom units remains speculative. Possible relationship between the climatic conditions, environmental events, human activities and magnetic record in the time span with preserved original iron oxides is depicted schematically in Fig. 12.

The high-resolution record in the point bar sequence shows increased magnetic signal in silty deposits containing the fine grained soil material eroded from fields (Fig. 7). Based on discrete flood resolution, the highest concentration of magnetic iron oxides reflects increased industrial pollution of the Morava R. catchment between 1972 and 1985. This could be related to acceleration of development of heavy industry and iron smelting complexes located at the Czech/Polish border, which are long-term sources of heavy pollution affecting large regions in the eastern part of the Czech Republic (Antušáková, 2013).

6. Conclusions

The Morava River floodplain architecture in the Strážnické Pomoraví area (Czech Republic) is characterized by alternating aggradation and degradation cycles since the Late Glacial. Up to five aggradation units

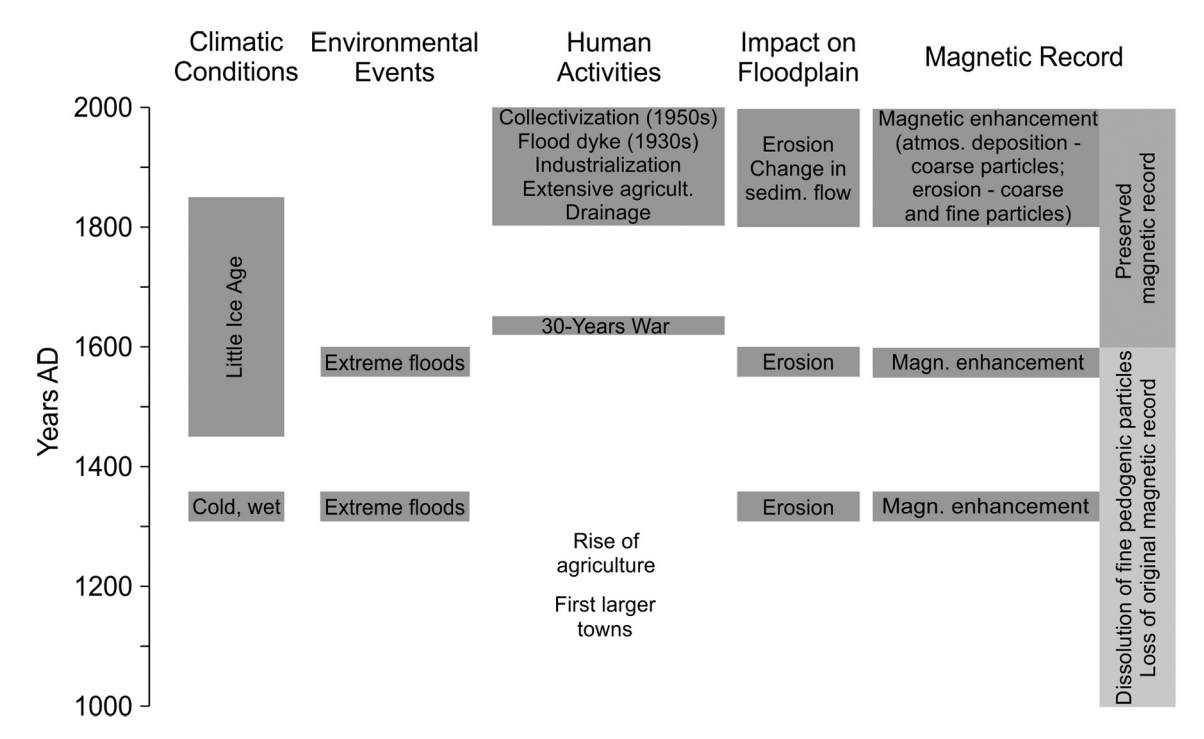


Fig. 12. Scheme of the main outcome of the study - relationship between different factors affecting the floodplain sediments and their possible magnetic record.

were recognized. The exposed river bank shows sediments deposited mostly during last millennium. Timing of the floodplain evolution using radiocarbon dating approach was often complicated by the redeposition and re-sedimentation of organic material. Only tree stumps or reed-mace roots preserved in situ offered credible ages. The high-resolution flood records were found in the point bar sequence formed since canalizing the Morava R. channel.

Only limited period of sediment deposition is available for reliable magnetic investigation (Units 4 and 5). Despite that, magnetic variations reveal continuous increase of ferrimagnetic minerals (magnetite/ maghemite) input to the floodplain. Frequency-dependent susceptibility does not prove unambiguously that magnetic enhancement in the uppermost layer is due to superparamagnetic magnetite of pedogenic origin. Even though, this enhancement may be related to the soil erosion in the Morava R. catchment. Although our data in general do not reflect a detailed record of individual floods, we can observe features that can be related to human activities. Moreover, reliable dating of individual events is obstructed by redeposition of sediments during floods. The most recent flood deposits are concentrated between flood dykes, constructed at the end of the 1930s. The erosion accelerated since the 1950s due to incorrect land use and the introduction of the corresponding agriculture techniques. The industrial pollution significantly contributes to the magnetic enhancement of the topmost 50 cm of the floodplain sequences.

Despite the local character of the study, we may draw a general conclusion that the records of paleoenvironmental changes and human activities in floodplain sediments may not be well preserved in all the strata. Moreover, the spatial distribution of individual markers may show significant variability, which may complicate cross-correlation even between sites very close to each other (in our case separated by flood dyke). However, from the point of view of future studies, the clastic floodplain sediments exposed along the Morava R. channel in the Strážnické Pomoraví area are suitable for high-resolution pollution and environmental studies covering mostly last century and especially period since 1950 to present-day.

Declaration of Competing Interest

The authors declare that they have no known competing financial interests or personal relationships that could have appeared to influence the work reported in this paper.

Acknowledgements

This work is to commemorate the first author, who suddenly passed away in 2020. We thank J. Diehl and S. Beske Diehl from the Michigan Technological University in Houghton for their advices on the manuscript and kind supervision during the NSF-NATO Post-Doctoral Fellowship of JK. Constructive comments of two anonymous reviewers and the editor P. Hesse are greatly appreciated. The research project was supported in the frame of the NSF-NATO Post-Doctoral Fellowship (No. DGE-0411426), by the Visiting Fellowship Program of the Institute for Rock Magnetism, University of Minnesota, by the Grant Agency CAS (IAAX00130801), by the Ministry of Education, Youth and Sports of the Czech Republic (MEYS) Operational Program Research, Development and Education Grant No. CZ.02.1.01/0.0/0.0/16_019/0000728, by the MEYS Inter-Vector project LTV19011, by the MEYS INTER-EXCEL-LENCE project LTC19029, and by the MEYS CzeCOS project LM2018123.

Appendix A. Supplementary data

Supplementary data to this article can be found online at https://doi.org/10.1016/j.palaeo.2022.111000.

References

- Antušáková, M., 2013. Historie a současnost ostravského průmyslu (History and the present of Ostrava industry). BSc. Thesis. Masaryk University, Brno, Czech Republic (49p. in Czech).
- Bábek, O., Fámēra, M., Hilscherová, K., Kalvoda, J., Dobrovolný, P., Sedláček, J., Machát, J., Holoubek, I., 2011. Geochemical traces of flood layers in the fluvial sedimentary archive; implications for contamination history analyses. Catena 87, 281–290.
- Bábek, O., Sedláček, J., Novák, A., Létal, A., 2018. Electrical resistivity imaging of anastomosing river subsurface stratigraphy and possible controls of fluvial style change in a graben-like basin. Czech Republic. Geomorphology 317, 139–156.
- Bloemendal, J., King, J., Hall, F.R., Doh, S.-J., 1992. Rock magnetism of late Neogene and Pleistocene deep-sea sediments: relationship to sediment source, diagenetic processes, and sediment lithology. J Geophys. Res. 97, 4361–4375. https://doi.org/ 10.1029/91JB03068.
- Bork, H.R., 1989. Soil erosion during the past millennium in central Europe and its significance within the geomorphodynamics of the Holocene. Catena Supplement 15, 121–131.
- Brázdil, R., Řezníčková, L., Máčka, Z., Valášek, H., Havlíček, M., Soukalová, E., Řehánek, T., Skokanová, H., 2011a. Fluctuations of floods of the River Morava (Czech Republic) in the 1691–2009 period: interactions of natural and anthropogenic factors. Hydrol. Sci. J. 56, 468–485.
- Brázdil, R., Máčka, Z., Řezníčková, L., Soukalová, E., Dobrovolný, P., Grygar, T.M., 2011b. Floods and floodplain changes of the River Morava, the Strážnické Pomoraví region (Czech Republic) over the past 130 years. Hydrol. Sci. J. 56, 1166–1185.
- Chaparro, M.A.E., Chaparro, M.A.E., Rajkumar, P., Ramasamy, V., Sinito, A.M., 2011. Magnetic parameters, trace elements, and multivariate statistical studies of river sediments from southeastern India: a case study from the Vellar River. Environ. Earth. Sci. 63, 297–310.
- Chaparro, M.A.E., Suresh, G., Chaparro, M.A.E., Ramasamy, V., Sinito, A.M., 2013. Magnetic studies and elemental analysis of river sediments: a case study from the Ponnaiyar River (Southeastern India). Environ. Earth. Sci. 70, 201–213. https://doi. org/10.1007/s12665-012-2116-y.
- Chaparro, M.A.E., Krishnamoorthy, N., Chaparro, M.A.E., Lecomte, K.L., Mullainathan, S., Mehra, R., Sinito, A.M., 2015. Magnetic, chemical and radionuclide studies of river sediments and their variation with different physiographic regions of Bharathapuzha River, southwestern India. Stud. Geophys. Geod. 59, 438–460. https://doi.org/10.1007/s11200-014-0145-6.
- Charleton, R., 2008. Fundamentals of Fluvial Geomorphology. Routledge (234p).
 Chudanicová, M., Hutchinson, S.M., 2016. Magnetic signature of overbank sediment in industry impacted floodplains identified by data mining methods. Geophys. J. Int. 207 (2), 1106–1121.
- Chudaničová, M., Hutchinson, S.M., Hradecký, J., Sedláček, J., 2016. Environmental magnetism as a dating proxy for recent overbank sediments of (peri-)industrial regions in the Czech Republic and UK. Catena 142, 21–35.
- Cook, E.R., Kairiūkštis, L.A., 1990. Methods of Dendrochronology Applications in the Environmental Sciences. In: Kluwer Academic Publisher and International Institute for Applied Systems Analysis (394p).
- Cook, E.R., Peters, K., 1981. The smoothing spline: a new approach to standardizing forest interior tree-ring width series for dendroclimatic studies. Tree Ring Bulletin 41, 45–53.
- Curie, L.A., 1995. Nomenclature in evaluation of analytical methods including detection and quantification capabilities. (IUPAC Recommendation 1995). Pure Appl. Chem. 67, 1699–1723.
- Czernik, J., Goslar, T., 2001. Preparation of graphite targets in the Gliwice radiocarbon laboratory for AMS 14C dating. Radiocarbon 43 (2A), 283–291.
- Day, R., Fuller, M., Schmidt, V.A., 1977. Hysteresis properties of titanomagnetites grain-size and compositional dependence. Phys. Earth Planet. Inter. 13, 260–267.
- Dearing, J.A., Hakansson, H., Liedbergjonsson, B., Persson, A., Skansjo, S., Widholm, D., Eldaoushy, F., 1987. Lake-sediments used to quantify the erosional response to landuse change in southern Sweden. Oikos 50, 60–78. https://doi.org/10.2307/ 3565402
- Dearing, J.A., Dann, R.J.L., Hay, K., Lees, J.A., Loveland, P.J., Maher, B.A., O'grady K., 1996. Frequency-dependent susceptibility measurements of environmental materials. Geophys. J. Int. 124, 228–240. https://doi.org/10.1111/j.1365-246X 1996 tb06366 x
- Dekkers, M.J., 1997. Environmental magnetism: an introduction. Geologie en Mijnbouw 76, 163–182.
- Ding, Z.L., Derbyshire, E., Yang, S.L., Yu, Z.W., Xiong, S.F., Liu, T.S., 2002. Stacked 2.6-Ma grain size record from the Chinese loess based on five sections and correlation with the deep-sea δ¹⁸O record. Palaeocenography 17 (3). https://doi.org/10.1029/2001PA000725.
- Dunlop, D.J., Özdemir, Ö., 1997. Rock Magnetism: Fundamentals and Frontiers. Cambridge University Press, Cambridge, U.K.
- Evans, M.E., Heller, F., 2004. Environmental magnetism. Academic Press, Principles and applications of Enviromagnetics, p. 299p.
- Fabian, K., Shcherbakov, V.P., McEnroe, S.A., 2013. Measuring the Curie temperature. Geochem. Geophys. Geosyst. 14 https://doi.org/10.1029/2012GC004440.
- Fáměra, M., Bábek, O., Grygar, T.M., Nováková, T., 2013. Distribution of heavy-metal contamination in regulated river-channel deposits: a magnetic susceptibility and grain-size approach; river Morava. Czech Republic. Water Air Soil Pollut. 224 https://doi.org/10.1007/s11270-013-1525-1.
- Flanders, P.J., 1994. Collection, measurement, and analysis of airborne magnetic particulates from pollution in the environment. J. Appl. Phys. 75, 5931–5936. https://doi.org/10.1063/1.355518.

- Franke, C., Patault, E., Alary, C., Abriak, N.E., Lagroix, F., 2020. Magnetic fingerprinting of fluvial suspended particles in the context of soil erosion: example of the Canche River watershed (Northern France). Geochem. Geophys. Geosyst. 21 https://doi.org/ 10.1029/2019GC008836.
- Frankl, A.L., Maxbauer, D.P., Savina, M.E., 2021. Linkages between soil organic matter and magnetic mineral formation in agricultural fields in southeastern Minnesota, USA. Geoderma 406, 115466. https://doi.org/10.1016/j.geoderma.2021.115466.
- Fritts, H.C., Mosimann, J.E., Bottorff, C.P., 1969. A revised computer program for standardizing tree–ring series. Tree Ring Bulletin 29, 15–20.
- Grissino-Mayer, H.D., Holmes, R., Fritts, H.C., 1992. International Tree-ring Data Bank Program Library. Version 1.1. Laboratory of Tree-Ring Research, University of
- Grygar, T., Světík, I., Lisá, L., Koptíková, L., Bajer, A., Wray, D.S., Ettler, V., Mihaljevič, M., Nováková, T., Koubová, M., Novák, J., Máčka, Z., Smetana, M., 2010. Geochemical tools for the stratigraphic correlation of floodplain deposits of the Morava River in Strážnické Pomoraví, Czech Republic from the last millennium. Catena 80, 106–121.
- Grygar, T.M., Nováková, T., Mihaljevič, M., Strnad, L., Světlík, I., Koptíková, L., Lisá, L., Brázdil, R., Máčka, Z., Stachoň, Z., Svitavská-Svobodová, H., Wray, D.S., 2011. Surprisingly small increase of the sedimentation rate in the floodplain of Morava River in the Strážnice area, Czech Republic, in the last 1300 years. Catena 86, 192–207.
- Grygar, T.M., Sedláček, J., Bábek, O., Nováková, T., Strnad, L., Mihaljevič, M., 2012. Regional contamination of Moravia (south-eastern Czech Republic): Temporal shift of Pb and Zn loading in fluvial sediments. Water Air Pollut. 223, 739–753.
- Grygar, T.M., Elznicová, J., Tůmová, S., Faměra, M., Balogh, M., Kiss, T., 2016. Floodplain architecture of an actively meandering river (the Ploucnice River, the Czech Republic) as revealed by the distribution of pollution and electrical resistivity tomography. Geomorphology 254, 41–56.
- Gupta, S.K., Polach, H.A., 1985. Radiocarbon Dating Practises at ANU. Radiocarbon Laboratory, Research School of Pacific Studies, ANU, p. 173p.
- Havlíček, P., Šmolíková, L., 1994. Evolution of south Moravian flood plains. Věstník Českého geologického ústavu 69, 23–40 (in Czech).
- Havlíček, P., Adámek, J., Adamová, M., Břízová, E., Bubík, M., Čtyroká, J., Čtyroký, P., Macek, J., Nekovařík, Č., Neudert, O., Novák, Z., Nováková, D., Petrová, P., Skácelová, Z., Stráník, Z., Šikula, J., Švábenická, L., 2007. Vysvětlivky k základní geologické mapě České republiky 1:25,000, list 34–224 Strážnice, 34–242 Mlýnky (Notes to the basic geological map of the Czech Republic 1:25,000, sheets 34–224 Strážnice, 34–242 Mlýnky. Czech Geological Survey, Prague) (57p. in Czech).
- Holmes, R.L., Adams, R.K., Fritts, H.C., 1986. In: Users Manual for Program ARSTAN. Tree-ring Chronologies of Western North America: California, Eastern Oregon and Northern Great Basin. Laboratory of Tree–Ring Research, University of Arizona, Tucson. AZ. pp. 50–56.
- Kadlec, J., Diehl, J.F., 2005. Magnetic properties of floodplain deposits along the banks of the Morava River (Czech Republic). IRM Quart 5 (3), 2–3.
- Kadlec, J., Grygar, T., Světlík, I., Ettler, V., Mihaljevič, M., Diehl, J.F., Beske-Diehl, S., Svitavská-Svobodová, H., 2009. Morava River floodplain development during the last millennium, Strážnické Pomoraví, Czech Republic. The Holocene 19, 499–509.
- Kalicki, T., 2006. Zapis zmian klimatu oraz działalności człowieka i ich rola w holoceńskiej ewolucji dolin środkowoeuropejskich (Reflection of climatic changes and human activity and their role in the Holocene evolution of Central European valleys). In: Prace Geograficzne IGIPZ PAN, 348p (in Polish).
- Kalicki, T., Krapiec, M., 1995. Problems of dating alluvium using buried subfossil tree trunks: lessons from the "black oaks" of the Vistula Valley. Central Europe. The Holocene 5 (2), 243–260.
- Kapička, A., Petrovský, E., Jordanova, N., Podrázský, V., 2001. Magnetic parameters of forest top soils in Krkonose Mountains. Czech Republic. Phys. Chem. Earth A 26, 917–922
- Kapička, A., Jordanova, N., Petrovský, E., Podrázský, V., 2003. Magnetic study of weakly contaminated forest soils. Water Air Soil Pollut. 148, 31–44.
- Knab, M., Hoffmann, V., Petrovský, E., Kapička, A., Jordanova, N., Appel, E., 2006. Surveying the anthropogenic impact of the Moldau river sediments and nearby soils using magnetic susceptibility. Environ. Geol. 49, 527–535.
- Kolář, T., Rybníček, M., Kyncl, T., 2012. The new oak standard chronology for the Czech Republic and its teleconnection on a European scale. Dendrochronologia 33 (3), 243–248.
- Liu, T.S., Ding, Z.L., 1998. Chinese loess and the palaeomonsoon. Annu. Rev. Earth Planet. Sci. 26, 111–145.
- Liu, Q., Roberts, A.P., Larrasoaña, J.C., Banerjee, S.K., Guyodo, Y., Tauxe, L., Oldfield, F., 2012. Environmental magnetism: Principles and applications. Rev. Geophys. 50, RG4002. https://doi.org/10.1029/2012RG000393.
- Máčka, Z., Kadlec, J., 2016. Strážnicke Pomoraví Holocene evolution of a unique floodplain and aeolian landforms. In: Pánek, T., Hradecký, J. (Eds.), Landscapes and Landforms of the Czech Republic. World Geomorphological Landscapes. Springer, pp. 361–371.
- Rumsby, B.T., Macklin, M.G., 1996. River response to the last neoglacial (the "Little Ice Age") in northern, western and central Europe. Geological Society, London, Special Publications 115, 217–233.
- Magiera, T., Jablonska, M., Strzyszcz, Z., Rachwal, M., 2011. Morphological and mineralogical forms of technogenic magnetic particlesin industrial dust. Atmos Environ. 45, 4281–4290.
- Maher, B.A., 1998. Magnetic properties of modern soils and Quaternary loessic paleools: paleoclimatic implications. Palaeogeogr. Palaeoclimat. Palaeoecol. 137, 25–54.
- Maher, B.A., 2007. Environmental magnetism and climate change. Contemp. Phys. 48 (5), 247–274.

- Maher, B.A., 2011. The magnetic properties of Quaternary aeolian dusts and sediments, and their palaeoclimatic significance. Aeolian Res. 3 (2), 87–144.
- Maher, B.A., Moore, C., Matzka, J., 2008. Spatial variation in vehicle-derived metal pollution identified by magnetic and elemental analysis of roadside tree leaves. Atmos. Environ. 42, 364–373.
- Nehyba, S., Adamová, M., Faimon, J., Kuchovský, T., Holoubek, I., Zeman, J., 2010a. Modern fluvial sediment provenance and pollutant tracing: a case study from the Dřevnice River Basin (eastern Moravia, Czech Republic). Geol. Carpat. 61 (2), 147–162.
- Nehyba, S., Hilscherová, K., Jarkovský, J., Dušek, L., Kuchovský, T., Zeman, J., Klánová, J., Holoubek, I., 2010b. Grain size, geochemistry and organic pollutants in modern fluvial deposits in eastern Moravia (Czech Republic). Environ. Earth Sci. 591–602.
- Nováková, T., Grygar, T.M., Bábek, O., Fáměra, M., Mihaljevic, M., Strnad, L., 2013. Distinguishing regional and local sources of pollution by trace metals and magnetic particles in fluvial sediments of the Morava River. Czech Republic. J. Soils Sedim. 13, 460-473.
- Oldfield, F., Barnosky, C., Leopold, E.B., Smith, J.P., 1983. Mineral magnetic studies of lake sediments. A brief review. Hydrobiologia 103 (1), 37–44.
- Oldfield, F., Gedye, A.A., Hunt, A., Jones, J.M., Jones, M.D.H., Richardson, N., 2015. The magnetic record of inorganic fly ash deposition in lake sediments and ombrotrophic peats. Holocene 25 (1), 215–225.
- Orsillo, N.P., 2008. Agricultural Intensification in Communist Czechoslovakia and its Impact on the Environment. MSc Thesis, Department of Environmental Studies, Faculty of Social Studies. Masaryk University, Brno, Czech Republic.
- Özdemir, Ö., Dunlop, D.J., Moskowitz, B.M., 1993. The effect of oxidation on the Verwey transition in magnetite. Geophys. Res. Lett. 20, 1671–1674. https://doi.org/10.1029/93GL01483.
- Pernes, J., 2016. Kolektivizace zemědělství v Československu v letech 1948–1960 (The Collectivisation of Agriculture in Czechoslovakia in the Years 1948–1960). Forum Historiae 10, 5–34 (in Czech with English abstract).
- Peters, C., Dekkers, M.J., 2003. Selected room temperature magnetic parameters as a function of mineralogy, concentration and grain size. Phys. Chem. Earth 28, 16–19. https://doi.org/10.1016/S1474-7065(03)00120-7.
- Petrovský, E., Kapička, A., 2006. On determination of the Curie point from thermomagnetic curves. J. Geophys. Res.-Solid Earth 111. https://doi.org/10.1029/ 2006JB004507.
- Pilařová, Z., 2008. Historické a současné povodně na řece Moravě a jejich dopady na ukládání sedimentů v oblasti Strážnickéh Pomoraví (Historical and recent floods on the Morava river and their impacts on sediment deposition in the region "Strážnické Pomoraví"). MSc. Thesis. Masaryk University, Brno, Czech Republic, 91p (in Czech).
- Platzman, E.S., Lund, S.P., 2019. High-resolution environmental magnetic study of a Holocene sedimentary record from Zaca Lake, California. The Holocene 29 (1), 17–25.
- Poláček, L., 2000. Terénní výzkum v Mikulčicích. Mikulčice-průvodce, sv. 1 (The Archaeology of Mikulčice. Mikulčice – Guide). Institute of Archaeology of the CAS, Brno, Czech Republic, 44p (in Czech).
- Poláček, L., 2007. Die Rolle der südmährischen Flüsse in der Geshichte Großmährens. In: Biermann, F., Kersting, T. (Eds.), Siedlung, Kommunikation und Wirtschaft im westslawischen Raum. Beiträge der Sektion zur slawischen Frühgeschichte des 5. Deutschen Archäologenkongresses in Frankfurt an der Oder, 4. bis 7. April 2005 (Langenweissbach 2007) 67–78. (in German).
- Prokop, O., Kolář, T., Kyncl, T., Rybníček, M., 2017. Updating the Czech millennia-long oak tree-ring width chronology. Tree Ring Res. 73 (1), 47–52. https://doi.org/10.3959/1536-1098-73.147.
- Ramsey, C.B., 2009. Bayesian analysis of radiocarbon dates. Radiocarbon 51 (1), 337–360.
- Ramsey, C.B., Lee, S., 2013. Recent and Planned Developments of the Program OxCal. Radiocarbon 55 (2–3), 720–730.
- Reimer, P.J., Austin, W.E.N., Bard, E., Bayliss, A., Blackwell, P.G., Bronk, Ramsey C., Butzin, M., Cheng, H., Edwards, R.L., Friedrich, M., Grootes, P.M., Guilderson, T.P., Hajdas, I., Heaton, T.J., Hogg, A.G., Hughen, K.A., Kromer, B., Manning, S.W., Muscheler, R., Palmer, J.G., Pearson, C., van der Plicht, J., Reimer, R.W., Richards, D.A., Scott, E.M., Southon, J.R., Turney, C.S.M., Wacker, L., Adolphi, F., Büntgen, U., Capano, M., Fahrni, S.M., Fogtmann-Schulz, A., Friedrich, R., Köhler, P., Kudsk, S., Miyake, F., Olsen, J., Reinig, F., Sakamoto, M., Sookdeo, A., Talamo, S., 2020. The IntCal20 Northern Hemisphere radioarbon age calibration curve (0–55 cal kBP). Radiocarbon 62 (4), 725–757.
- Rybníček, M., Vavrčík, H., Hubený, R., 2006. Determination of the number of sapwood annual rings in oak in the region of southern Moravia. J. Forest Sci. 52 (3), 141–146.
- Rybníček, M., Koňas, P., Kolář, T., 2010. The benefits of tree-ring curves detrending for dating archaeological wood. Geochronometria 35 (1), 85–90.
- Sandeep, K., Shankar, R., Krishnaswamy, J., 2011. Assessment of suspended particulate pollution in the Bhadra River catchment, Southern India: an environmental magnetic approach. Environ. Earth Sci. 62, 625–637.
- Schweingruber, F.H., 1983. Der Jahrring: Standort, Methodik, Zeit und Klima in der Dendrochronologie. Paul Haupt Verlag, Bern, Switzerland (in German).
- Sedláček, J., Bábek, O., Grygar, T.M., 2013. Trends and evolution of contamination in a well-dated water reservoir sedimentary archive: the Brno Dam, Moravia, Czech Republic. Environ. Earth. Sci. 69, 2581–2593.
- Sedláček, J., Kapustová, V., Šimíček, D., Bábek, O., Sekanina, M., 2019. Initial stages and evolution of recently abandoned meanders revealed by multi-proxy methods in the Odra River (Czech Republic). Geomorphology 333, 16–29.
- Šmelko, Š., Wolf, J., 1977. Štatistické metódy v lesníctve (Statistical Methods in Forestry). Príroda, Bratislava, Slovakia, 330p (in Slovak).

- Smetana, M., 2011. Dynamika koryta Moravy ve vztahu k příbřežní vegetaci na základě studia historických map a současných měření: případová studie ze Strážnického Pomoraví (Dynamics of the River Morava changes in relation to riparian vegetation based on the study of old maps and contenporary measurements: case study from Strážnické Pomoraví). Zprávy o geologických výzkumech na Moravě a ve Slezsku. 18 (2), 58–63 (in Czech).
- Stuiver, M., Polach, H.A., 1977. Reporting of 14C data. Radiocarbon 19, 355-363.
- Sundman, A., Byrne, J.M., Bauer, I., Menguy, N., Kappler, A., 2017. Interactions between magnetite and humic substances: redox reactions and dissolution processes.

 Geochem. Trans. 18 https://doi.org/10.1186/s12932-017-0044-1.
- Svoboda, J., Vašků, Z., Cílek, V., 2003. Velká kniha o klimatu zemí Koruny české (Great Book on Climate of the Czech Crown Countries). Regia, Prague, 655p (in Czech).
- Tauxe, L., Mullender, T.A.T., Pick, T., 1996. Potbellies, wasp-waists, and superparamagnetism in magnetic hysteresis. J. Geophys. Res.-Solid. Earth 101, 571–583
- Thompson, R., Oldfield, F., 1986. Environmental Magnetism. Allen & Unwin, p. 227p. Till, J.L., Nowaczyk, N., 2018. Authigenic magnetite formation from goethite and hematite and chemical remanent magnetization acquisition. Geophys. J. Int. 213, 1818–1831.
- Verosub, K.L., Roberts, A.P., 1997. Environmental magnetism: past, present, and future. J. Geophys. Res. 100, 2175–2192.
- Wang, G., Chen, J., Zhang, W., Chen, Y., Ren, F., Fang, A., Ma, L., 2019. Relationship between magnetic properties and heavy metal contamination of street dust samples from Shanghai. China. Environ. Sci. Pollut. Res. 26, 8958–8970.
- Zádorová, T., Penížek, V., Šefrna, L., Rohošková, M., Borůvka, L., 2011. Spatial delineation of organic carbon-rich Colluvial siols in Chernozem regions by Terrain analysis and fuzzy classification. Catena 22–33.
- Zhang, W., Dong, Ch., Hutchinson, S.M., Ge, C., Wang, F., Feng, H., 2018. Recent applications of mineral magnetic methods in sediment pollution studies: a review. Curr. Pollut. Rep. 4, 1–7.